Georgia State University
ScholarWorks @ Georgia State University

Chemistry Theses | Department of Chemistry

12-14-2021

# Mechanistic Characterization of Active Site Residues in Nitronate Monooxygenase from Pseudomonas aeruginosa PAO1

Christopher Aguillon
caguillon1@student.gsu.edu

Follow this and additional works at: https://scholarworks.gsu.edu/chemistry_theses

## Recommended Citation

Aguillon, Christopher, "Mechanistic Characterization of Active Site Residues in Nitronate Monooxygenase from Pseudomonas aeruginosa PAO1." Thesis, Georgia State University, 2021.
doi: https://doi.org/10.57709/26662742

This Thesis is brought to you for free and open access by the Department of Chemistry at ScholarWorks @ Georgia State University. It has been accepted for inclusion in Chemistry Theses by an authorized administrator of ScholarWorks @ Georgia State University. For more information, please contact scholarworks@gsu.edu.

# Mechanistic Characterization of Active Site Residues in Nitronate Monooxygenase from *Pseudomonas aeruginosa* PAO1

by

Christopher Aguillon

Under the Direction of Giovanni Gadda, PhD

A Thesis Submitted in Partial Fulfillment of the Requirements for the Degree of

Master of Science

in the College of Arts and Sciences

Georgia State University

2021

ABSTRACT

Propionate 3-nitronate (P3N) is a natural toxin that irreversibly inhibits the Krebs cycle – a life sustaining metabolic pathway. Nitronate monooxygenase detoxifies P3N using molecular oxygen. Among ~500 NMO sequences from various organisms, NMO has evolved to contain Y109, Y254, Y299, Y303, K307, and H183 in putative NMOs. In this thesis, the role of these select residues in the binding and oxidation of P3N is studied. Using steady state kinetics and UV-visible absorption spectroscopy, Y109, Y254, Y299, Y303, and K307 were found to have no role in the turnover of P3N. Utilizing steady-state, rapid kinetics, and x-ray crystallography, H183 was determined to be an essential residue in binding P3N into an enzyme-substrate complex competent for the single electron transfer between P3N and the reactive center of the enzyme.

INDEX WORDS: Conformational change, Electron transfer, Enzyme catalysis, Flavin mononucleotide (FMN), Glutamine, Histidine, Isomerization, Mutagenesis, Oxidation-reduction, Structure-function

Copyright by
Christopher Camacho Aguillon
2021

Mechanistic Characterization of Active Site Residues in Nitronate Monooxygenase from *Pseudomonas aeruginosa* PAO1

by

Christopher Aguillon

Committee Chair: Giovanni Gadda

Committee: Dabney Dixon

Donald Hamelberg

Electronic Version Approved:

Office of Graduate Services

College of Arts and Sciences

Georgia State University

December 2021

## DEDICATION

*To my mother Carolina Camacho Aguillón.*

## ACKNOWLEDGEMENTS

I want to thank my research advisor Giovanni Gadda for his mentorship throughout my undergraduate career. Additionally, I want to thank all the Gadda lab members for their insightful suggestions and friendship I want to thank Archana Iyer, Daniel Ouedraogo, Renata Reis, Maria Vodovoz, and Benjamin Dratch.

I want to thank my family Carolina and Amaris Aguillon, and Iris Alvarez, Jacquelin and Mirna Camacho, and Mark, Abraham, and Marco Torres for their support and guidance.

I also want to thank my partner Billy W. Crosby, Jr for all his support and unconditional love.

The work of in this thesis was supported in part by Undergraduate Molecular Basis of Disease, Initiative for Maximizing Student Development (NIH R25GM109442), and Louis Stokes Alliance for Minority Participation Fellowships and a Maximizing Access to Research Careers assistantship (NIH T34GM131939).

# TABLE OF CONTENTS

## LIST OF TABLES

## LIST OF FIGURES

# 1 INTRODUCTION

## 1.1 Background

Nitronate monooxygenase (NMO; E.C. 1.13.12.16) is a flavin-dependent enzyme involved in the detoxification of alkyl nitronates. More specifically, propionate 3-nitronate (P3N) is a toxic compound oxidized by NMO using oxygen. P3N is found in nature in its acid form as a glycosylated compound. Upon ingestion, P3N can irreversibly inhibit complex II in the Kreb's Cycle – a life-sustaining biochemical pathway involved in energy production (1). Recently, *in vivo* studies demonstrated the protective nature of NMO against environmental P3N (2). These studies found that exogenous NMO aids in bacterial growth in the presence of P3N and its conjugate acid 3-nitropropionic acid (3-NPA). Additionally, a knock-out study demonstrated that a lack of an NMO gene inhibits the growth of *Neurospora crassa* in the presence of P3N/3-NPA (2).

NMOs are members of group H monooxygenases (3). These enzymes are characterized by having flavin mononucleotide (FMN) as a cofactor and a TIM-barrel fold. The biochemistry of this group of enzymes is characterized by a flavin reduction and a concomitant substrate oxidation as seen in the reaction of P3N and NMO. In NMO, flavin reduction occurs by a one-electron transfer from P3N yielding a flavosemiquinone. Then, the P3N radical or the flavosemiquinone activates molecular oxygen (4). In the turnover of NMO from *Pseudomonas aeruginosa* (*Pa*NMO), P3N is oxidized with a second-order rate constant of $10.8 \times 10^6$ $M^{-1}$ $s^{-1}$; NMOs from fungal sources such as *N. crassa* and *Cyberlindnera saturnus* (*Nc*NMO and *Cs*NMO) have second-order rate constants of $>10^6$ $M^{-1}$ $s^{-1}$ (5).

Over 4,000 genes are currently annotated as putative NMOs from various organisms. Of these, 475 sequences contain four distinct motifs of NMO coming from bacterial, fungal, and animal sources (5). The four motifs are based off the structure of *Pa*NMO for which functional and structural data exist. Among these putative NMOs, several key residues such as Y109, Y303, Y254, Y299, H133, and H183 are conserved. H183 is a fully conserved residue located on an active site loop 5.7 Å above FMN. H196 in *Nc*NMO is the homologous residue corresponding to H183 in *Pa*NMO. H196 was shown to act as a catalytic base that deprotonates the α-carbon of nitroethane to begin nitronate oxidation (6). The role for H196 in *Nc*NMO is not expected to be the same as H183 in *Pa*NMO or *Cs*NMO because the latter two enzymes only use nitronates as substrates and not their conjugate acids nitroalkanes (5). In other words, *Pa*NMO and *Cs*NMO cannot deprotonate the α-carbon of nitroalkanes to produce nitronates as seen in the catalytic strategy of *Nc*NMO. The side chain of H183 points towards the N5 atom of the flavin. In between H183 and the N5 atom, a water molecule serves as a bridge. It is postulated that the residue serves as a participant in arranging P3N in an enzyme-substrate complex suitable for the electron transfer reaction between P3N and the flavin.

## 1.2 Specific Aims

The thesis aims to investigate the role of the conserved residues Y109, Y254, Y299, Y303, K307, and H183 in nitronate monooxygenase (NMO). Among ～500 sequences, these residues have been conserved in putative NMOs. It is postulated that these residues participate in substrate binding and the oxidation of toxin propionate 3-nitronate (P3N). More specifically, it is hypothesized that the hydroxyl groups of each tyrosine or the amine group of K307 interact with the carboxylate group of the P3N substrate. Separately, the H183 is thought to bind P3N into an ES complex competent for the electron transfer reaction between P3N and the flavin cofactor.

Utilizing site-directed mutagenesis, steady state kinetics and UV-visible absorption spectroscopy, the role of Y109, Y254, Y299, Y303, and K307 in the binding and catalysis of P3N were determined. In the study of H183, site-directed mutagenesis, steady state kinetics, rapid kinetics, and x-ray crystallography were used to determine the interaction of H183 with the ES complex in NMO.

1. Coles, C. J., Edmondson, D. E., and Singer, T. P. (1979) Inactivation of succinate dehydrogenase by 3-nitropropionate. *J. Biol. Chem* .**254**, 5161-5167
2. Francis, K., Nishino, S. F., Spain, J. C., and Gadda, G. (2012) A novel activity for fungal nitronate monooxygenase: detoxification of the metabolic inhibitor propionate-3-nitronate. *Arch Biochem Biophys* **521**, 84-89
3. Huijbers, M. M. E., Montersino, S., Westphal, A. H., Tischler, D., and van Berkel, W. J. H. (2014) Flavin dependent monooxygenases. *Archives of Biochemistry and Biophysics* **544**, 2-17
4. Smitherman, C., and Gadda, G. (2013) Evidence for a Transient Peroxynitro Acid in the Reaction Catalyzed by Nitronate Monooxygenase with Propionate 3-Nitronate. *Biochemistry* **52**, 2694-2704
5. Salvi, F., Agniswamy, J., Yuan, H., Vercammen, K., Pelicaen, R., Cornelis, P., Spain, J. C., Weber, I. T., and Gadda, G. (2014) The combined structural and kinetic characterization of a bacterial nitronate monooxygenase from *Pseudomonas aeruginosa* PAO1 establishes NMO class I and II. *J Biol Chem* **289**, 23764-23775

6. Francis, K., and Gadda, G. (2008) The nonoxidative conversion of nitroethane to ethylnitronate in Neurospora crassa 2-nitropropane dioxygenase is catalyzed by histidine 196. *Biochemistry* **47**, 9136-9144

# 2 CHARACTERIZATION OF CONSERVED ACTIVE SITE RESIDUES IN CLASS I NITRONATE MONOOXYGENASE

(This chapter has been published verbatim in Su, D., Aguillon, C., and Gadda, G. (2019), Archives of Biochemistry and Biophysics 672 (2019) 1080582.)

## 2.1 Abstract

Propionate 3-nitronate (P3N) is a natural toxin that irreversibly inhibits mitochondrial succinate dehydrogenase. P3N poisoning leads to a variety of neurological disorders and even death. Nitronate monooxygenase (NMO) from *Pseudomonas aeruginosa* PAO1 was the first NMO characterized in bacteria and serves as a paradigm for Class I NMO. Here, we hypothesized that the carboxylate group of P3N might form a hydrogen bond with one or more of the four tyrosine or a lysine residues that are conserved in the active site of the enzyme. In the wild-type enzyme, the $k_{cat}$ value was pH independent between pH 6.0 and 11.0, while the $k_{cat}/K_{P3N}$ value decreased at high pH, suggesting that a protonated group with a p$K_a$ value of 9.5 is required for binding the anionic substrate. A pH titration of the UV-visible absorption spectrum of the enzyme showed an increased absorbance at 297 nm with increasing pH, defining a p$K_a$ value of 9.5 and a $\Delta\varepsilon_{297\ nm}$ of 2.4 $M^{-1}cm^{-1}$, consistent with a tyrosine being important for substrate binding. The N3 atom of the oxidized flavin, instead, did not ionize likely because its p$K_a$ was perturbed by the ionization of a tyrosine in the active site of the enzyme. The Y109F, Y254F, Y299F, Y303F, and K307M, substitutions had small effects (i.e., <3.5-fold) on the steady-state kinetic parameters of the enzyme. With all mutated enzymes, the $k_{cat}/K_{P3N}$ value was less than 2.5-fold different from the wild-type enzyme, suggesting that none of the residues is solely important for substrate binding.

## 2.2 Introduction

Nitronate monooxygenase (NMO, E.C. 1.13.12.16) is an FMN-dependent enzyme that uses molecular oxygen to oxidize propionate 3-nitronate (P3N) (4-7). P3N exists in equilibrium with 3-nitropropionic acid (3-NPA), which in plants (8,9), fungi (10,11), and insects(12,13), is stored in a number of glycosidic esters and is released upon acidic hydrolysis (9,14). P3N is a potent inhibitor of mitochondrial succinate dehydrogenase, resulting in ATP depletion and heightened oxidative stress (14,15). Livestock and human intoxication by P3N manifest in foaming of the mouth, respiratory distress, neurological impairment, and often times death (6,16,17). Two classes of NMOs have been established using a combination of biochemical and structural analyses, and bioinformatics (5). Class I NMO includes ~500 enzymes from bacteria, fungi, and two animals, including a biochemically characterized prokaryotic NMO from *Pseudomonas aeruginosa* PAO1 (*Pa*NMO) and a eukaryotic NMO from *Cyberlindnera saturnus* (*Cs*NMO) (5,7). Class II NMO comprises ~10 enzymes (5), and includes a biochemically characterized eukaryotic NMO from *Neurospora crassa* (*Nc*NMO) (6,18,19) .

The enzymatic oxidation of P3N in Class I NMO begins with a single electron transfer from P3N to the enzyme-bound FMN, forming a P3N radical species and a flavin semiquinone (4,5). *Pa*NMO is the only enzyme for which thermodynamic stabilization of both neutral and anionic semiquinones with a ratio that is pH-dependent has been demonstrated to date (20). The P3N radical is proposed to react directly with molecular oxygen to generate a 3-peroxy-3-nitropropanoate radical. A subsequent electron transfer from the flavin semiquinone to the 3-peroxy-3-nitropropanoate radical gives 3-peroxy-3-nitropropanoate, which would decay to the products. Alternatively, the flavin semiquinone

would donate an electron to molecular oxygen yielding superoxide anion, which subsequently reacts with P3N radical to form 3-peroxy-3-nitropropanoate. Consistent with the reductive and oxidative half-reactions involving single electron transfers, the steady-state kinetic parameters $k_{cat}/K_{P3N}$ and $k_{cat}/K_{O2}$ are unusually large for a flavin-dependent monooxygenase, with values in the $10^6$-$10^7$ $M^{-1}s^{-1}$ range (4,5). Enzyme turnover at saturating concentrations of P3N and oxygen is also fast with a $k_{cat}$ value of 1,300 $s^{-1}$ at pH 7.5 and 30 $^oC$ (4,5). The crystallographic structures of *Pa*NMO and *Cs*NMO have been solved previously to resolutions ≤1.65 Å (5,7), demonstrating a collection of fully conserved residues in the active site of the prokaryotic and eukaryotic enzymes. While the available structures provide a platform to hypothesize roles for active site residues, no mutagenesis studies have been reported to establish which amino acid residues participate in substrate binding and catalysis.

In the active site of Class I NMO there are three fully conserved tyrosine residues, Y109, Y299, and Y303 (numbering for *Pa*NMO) (Figure 1). A fourth tyrosine is conserved in ~70% of the amino acid sequences, being replaced with a histidine in ~25% of the sequences and phenylalanine and tryptophan in the remaining cases. Another fully conserved residue in Class I NMO is K307, which is located at the entrance of the active site. It is conceivable that at least one or more of these residues participate as a hydrogen bond donor for binding the carboxylate group of the P3N substrate. Thus, we hypothesize that the individual replacement of a conserved active site tyrosine residue(s) with a phenylalanine or the lysine residue with methionine would negatively impact substrate binding. In this study, we have used mutagenesis, steady-state kinetics on the mutant enzymes, and pH effects on the steady-state kinetic parameters and the UV-visible

absorption spectrum of the wild-type enzyme to establish which, if any, of the conserved amino acid residues in the active site of Class I NMO is important for binding the P3N substrate.

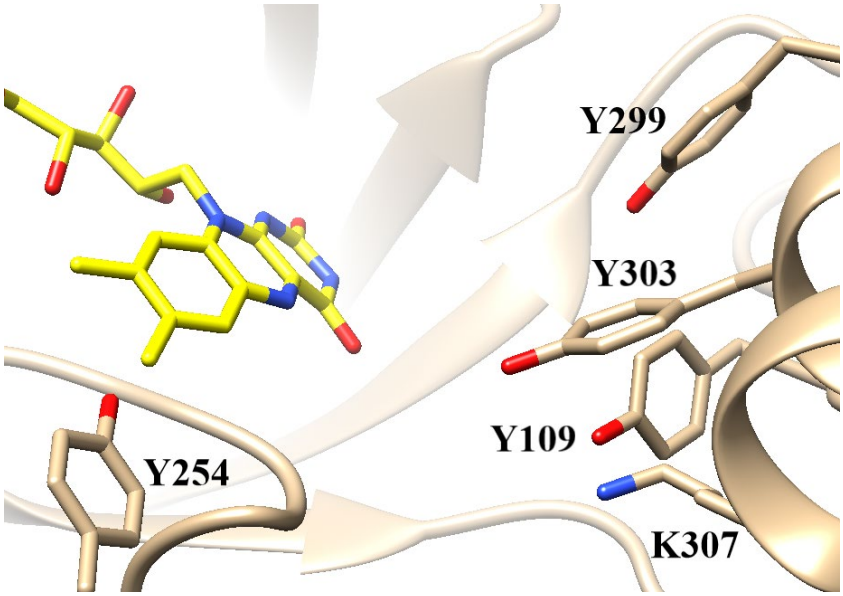


*Figure 2.1 Conserved active site residues in PaNMO (PDB entry 4Q4K). The carbon atoms of the FMN cofactor are shown as yellow sticks, whereas those of select protein residues are displayed as tan sticks; nitrogen and oxygen atoms are colored in blue and red, respectively.*

## 2.3 Materials and Methods

### *2.1 Site-Directed Mutagenesis and Purification of PaNMO variants*

The genes for nitronate monooxygenase variants Y109F, Y254F, Y299F, Y303F, and K307M were prepared using the pET20b(+) plasmid harboring the wild-type gene PA4202 as a template and mutagenic primers containing the corresponding site mutation. Upon mutagenesis, the mutant genes were sequenced at Macrogen Inc (Rockville, MD). Plasmids were purified using kits from Qiagen Inc. (Valencia, CA). The constructs

containing the correct mutation were transformed by heat shock into *Escherichia coli* strain Rosetta(DE3)pLysS competent cells for protein expression (21). The expression and purification of NMO mutant enzymes Y109F, Y254F, Y299F, Y303F, and K307M, followed the protocol of wild-type enzyme as previously described (5).

### *2.2 Enzymatic assays*

3-Nitropropionic acid was from Sigma-Aldrich (St. Louis, MO). Similar to primary and secondary nitroalkanes, the α-carbon atom of 3-nitropropionic acid has a p$K_a$ value of 9.1 and undergoes slow deprotonation with a strong base (22). P3N, the conjugate base of 3-nitropropionic acid, was thus prepared in water by incubating the nitro compound with a 2.2 molar excess of KOH for 24 h at 4 $^{o}$C, as previously described (4,5). Addition of KOH was slow to avoid sample boiling and possible decomposition of P3N, which was then used within a week (23).

Enzymatic activity was measured by monitoring initial rates of oxygen consumption using a computer-interfaced Oxy-32 oxygen-monitoring system (Hansatech Instruments, Inc., Norfolk, England). The steady-state kinetic parameters for wild-type and variant enzymes were obtained by varying concentrations of P3N and oxygen. The experiment was carried out in the presence of 50 mM potassium phosphate at pH 8.0 and 30 $^{o}$C. The assay reaction mixture was equilibrated with an $O_2/N_2$ gas mixture to reach a desired oxygen concentration for at least 5 min before initiating the reaction with the addition of enzyme then P3N. Since the second-order rate constants for protonation of the nitronates are in the range 15-75 $M^{-1}s^{-1}$ (24,25), enzymatic activity assays were initiated with the addition of the nitronate to the reaction mixture to ensure that a negligible amount of the

neutral species of the nitronate was present during the time required to acquire initial rates of reaction (typically ~30 s). The pH dependence of the steady-state kinetic parameters of the wild-type enzyme were determined as described above in the pH range between 6.0 and 11.0, with the exception of pH 8.0 where 50 mM sodium phosphate was used.

### *2.3 UV-visible absorption spectroscopy*

UV-visible absorption spectra were recorded using an Agilent Technologies model HP 8453 PC diode-array spectrophotometer (Santa Clara, CA). The extinction coefficients of the enzyme-bound FMN for the variant enzymes were determined by heat denaturation (26). The enzymes were passed through a PD-10 desalting column equilibrated with 50 mM potassium phosphate at pH 7.0, before heat denaturation at 100 °C for 30 or 40 min. The denatured protein was removed by centrifugation at 20,000 × *g*, and the concentration of released FMN was measured using a molar extinction coefficient $\varepsilon_{450\ nm}$ of 12,200 $M^{-1}$ $cm^{-1}$ for free FMN (27). The total protein concentration was determined by using the Bradford assay with bovine serum albumin as standard (28). For the pH dependence of the UV-visible absorption spectrum, the wild-type enzyme was passed through a PD-10 desalting column equilibrated with 20 mM sodium phosphate and 20 mM sodium pyrophosphate, pH 7.8. A 2-mL enzyme solution with a concentration of enzyme-bound FMN of 10 μM was used to record the absorption spectra. Serial additions of 1-10 μL of 1 M NaOH were carried out into the enzyme solution with a 10 μL syringe while stirring until the pH was incrementally changed to ~10.4. After each careful

and slow addition of the base the enzyme solution was let equilibrate until no changes in the pH value and absorbance were observed, which typically required 2-3 min.

### *2.4 Data analysis*

Steady-state kinetic data were fit using KaleidaGraph software (Synergy Software, Reading, PA) or Enzfitter (Biosoft, Cambridge, UK) software. When initial rates of reaction were determined at varying concentrations of P3N and oxygen, the kinetic data were fit to Eqs 1 and 2. Eq 1 is for a sequential steady-state kinetic mechanism where $v_o$ represents the initial velocity, $e$ is the concentration of the enzyme, $k_{cat}$ is the first-order macroscopic rate constant for enzyme turnover at saturating concentration of both P3N and oxygen, $K_{P3N}$ and $K_{O2}$ are the Michaelis constants for P3N and oxygen, respectively, and $K_{ia}$ is a kinetic constant that accounts for the intersecting line pattern in the double reciprocal plot. Eq 2 represents a sequential steady-state kinetic mechanism of the type described by Eq 1 when $K_{ia}$ is not significantly different from zero. Data for each variant enzyme were fit to both equations and the equation providing the best fit ($R^2$) was used to determine the kinetic parameters.

The pH dependence of the $k_{cat}/K_{P3N}$ value for the wild-type enzyme was determined with Eq 3, which describes a pH profile with a limiting value ($C$) at low pH and a slope of -1 at high pH.

The pH dependence of the UV-visible absorption spectrum of the wild-type enzyme was fit to Eq 4, which describes a curve with one p$K_a$ value and two limiting values at high pH ($A$) and low pH ($B$).

$$\frac{v_o}{e} = \frac{k_{\text{cat}}[\text{P3N}][\text{O}_2]}{K_{\text{P3N}}[\text{O}_2] + K_{\text{O2}}[\text{P3N}] + [\text{P3N}][\text{O}_2] + K_{\text{ia}}K_{\text{O2}}} \quad (1)$$

$$\frac{v_o}{e} = \frac{k_{\text{cat}}[\text{P3N}][\text{O}_2]}{K_{\text{P3N}}[\text{O}_2] + K_{\text{O2}}[\text{P3N}] + [\text{P3N}][\text{O}_2]} \quad (2)$$

$$\log\left(k_{\text{cat}}/K_{\text{P3N}}\right) = \log\left(\frac{C}{1+10^{(pH-pK_a)}}\right) \quad (3)$$

$$Y = \frac{A+B\times10^{(pK_a-pH)}}{1+10^{(pK_a-pH)}} \quad (4)$$

## 2.4 Results

### *3.1 Purification and spectral properties of PaNMO variants*

The mutated enzymes Y109F, Y254F, Y299F, Y303F, and K307M, were purified to high levels following the same protocol previously used for the wild-type enzyme (5). The UV-visible absorption spectra of the variant enzymes showed the characteristic features of oxidized flavoproteins with maximal absorbance at ~370 nm and ~443 nm (Figure 2). All variant enzymes showed <10% differences in the absorption intensity at ~443 nm, and up to a 23%-increase in the absorption intensity at ~370 nm compared to the wild-type enzyme (Table 1). These changes agree well with an increase in the hydrophobicity of the protein environment surrounding the flavin introduced in the enzyme by the replacement of tyrosine and lysine with phenylalanine and methionine, respectively (29). In all cases the FMN/protein stoichiometry was low, but comparable with that of the wild-type enzyme purified from heterologous expression in *E. coli* (Table 1).

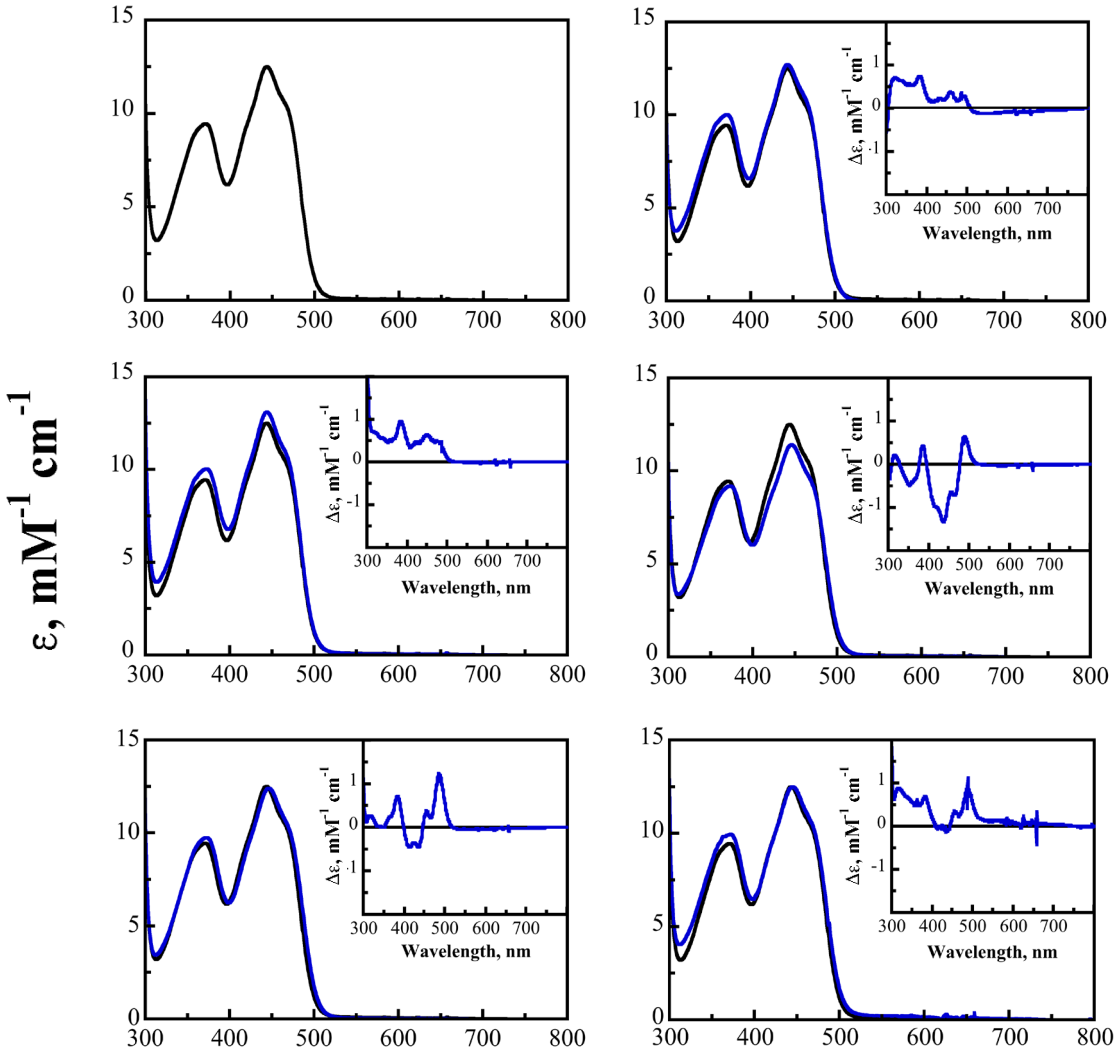


*Figure 2.2 UV-visible absorption spectra of wild-type and mutated PaNMO. The UV-visible absorption spectra were recorded in 50 mM potassium phosphate, pH 8.0. Enzymes: wild-type (A), Y109F (B), Y254F (C), Y299F (D Y303F (E), and K307M (F). Insets show the difference absorption spectra of variant enzyme minus the wild-type enzyme.*

*Table 2.1 UV-Visible Absorption Maxima and FMN/Protein Stoichiometry of Wild-Type and Mutated PaNMO*

| | WT | Y109F | Y254F | Y299F | Y303F | K307M |
|---|---|---|---|---|---|---|
| [a]$\lambda_{max}$, nm | 370, 443 | 371, 443 | 371, 443 | 372, 445 | 372, 446 | 370, 445 |
| [a]$\varepsilon$ ($mM^{-1}cm^{-1}$) | 8.4, 12.5 | 10, 12.7 | 10.3, 13.1 | 9.1, 11.4 | 9.7, 12.4 | 10, 12.5 |
| [b]FMN/protein | 0.25 | 0.21 | 0.17 | 0.16 | 0.16 | 0.14 |

[a] Spectra were recorded in 50 mM potassium phosphate, pH 8.0 and 15 °C.
[b] Molar ratio.

### *3.2 pH-Profiles of steady-state kinetic parameters for wild-type PaNMO*

The pH dependence of the steady-state kinetic parameters of the wild-type enzyme was determined to establish possible ionizations of active site residues involved in substrate binding and the half-reactions catalyzed by the enzyme. To this end, initial rates of reaction were determined with an oxygen electrode at varying concentrations of both P3N and oxygen in the pH range from 6.0 to 11.0, as illustrated in the example of Figure 3A. At all pH values tested, the best fit of the steady-state kinetic data was obtained with Eq 2, consistent with a value for the $K_{ia}$ constant being negligible when compared to the $K_{P3N}$ and $K_{O2}$ values (Table 2). As shown in Figure 3B, the $k_{cat}$ value was independent of pH with an average value of 1200 (±200) $s^{-1}$, consistent with no ionizable groups being involved in kinetic steps that determine the overall turnover of the enzyme saturated with both substrates. The $k_{cat}/K_{P3N}$ had a maximal value of 4.5 × $10^6$ (±1 × $10^6$) $M^{-1}s^{-1}$ up to pH 9.0 and decreased at higher pH values yielding a p$K_a$ value of 9.5 (±0.1), consistent with the requirement for a group to be protonated in the reductive half-reaction catalyzed by the enzyme (Figure 3B). In contrast, the $k_{cat}/K_{O2}$ value was pH-independent with an average value of 4.4 × $10^6$ (±2.7 × $10^6$) $M^{-1}s^{-1}$, consistent with absence of ionizable groups being relevant in the oxidative half-reaction catalyzed by the enzyme (Figure 3B). The

steady-state kinetic parameters of *Pa*NMO in the pH-independent region were comparable with those previously reported for eukaryotic *Cs*NMO, showing pH-independent values for $k_{cat}$ = 1,450 (±10) $s^{-1}$, $k_{cat}/K_{P3N}$ = 10.8 × $10^6$ (±0.2 × $10^6$) $M^{-1}s^{-1}$, and $k_{cat}/K_{O2}$ = 19.0 × $10^6$ (±0.3 × $10^6$) $M^{-1}s^{-1}$ (4).

*Table 2.2 Effects of pH on Steady-State Kinetic Parameters of Wild-Type PaNMO*

| pH | $k_{cat}/K_{P3N}$, $M^{-1}s^{-1}$ | $k_{cat}/K_{O2}$, $M^{-1}s^{-1}$ | $k_{cat}$, $s^{-1}$ | $K_{P3N}$, mM | $K_{O2}$, mM |
|---|---|---|---|---|---|
| 6.0 | 3.7 (±0.5) × $10^6$ | 4.2 (±0.6) × $10^6$ | 1500 (±20) | 0.41 (±0.01) | 0.36 (±0.01) |
| 7.0 | 4.2 (±0.3) × $10^6$ | 5.2 (±0.6) × $10^6$ | 1300 (±50) | 0.31 (±0.02) | 0.25 (±0.02) |
| 8.0 | 5.7 (±0.5) × $10^6$ | 10.0 (±1.2) × $10^6$ | 1200 (±100) | 0.21 (±0.01) | 0.12 (±0.01) |
| 9.0 | 3.0 (±0.4) × $10^6$ | 3.0 (±0.4) × $10^6$ | 1100 (±100) | 0.37 (±0.04) | 0.37 (±0.04) |
| 10.0 | 9.9 (±0.1) × $10^5$ | 4.1 (±0.2) × $10^6$ | 820 (±100) | 0.83 (±0.01) | 0.20 (±0.01) |
| 10.5 | 4.3 (±1.9) × $10^5$ | 1.7 (±0.9) × $10^6$ | 1300 (±400) | 3.0 (±1.0) | 0.77 (±0.36) |
| 11.0 | 1.2 (±0.1) × $10^5$ | 2.8 (±0.1) × $10^6$ | 1200 (±20) | 9.7 (±0.4) | 0.43 (±0.02) |

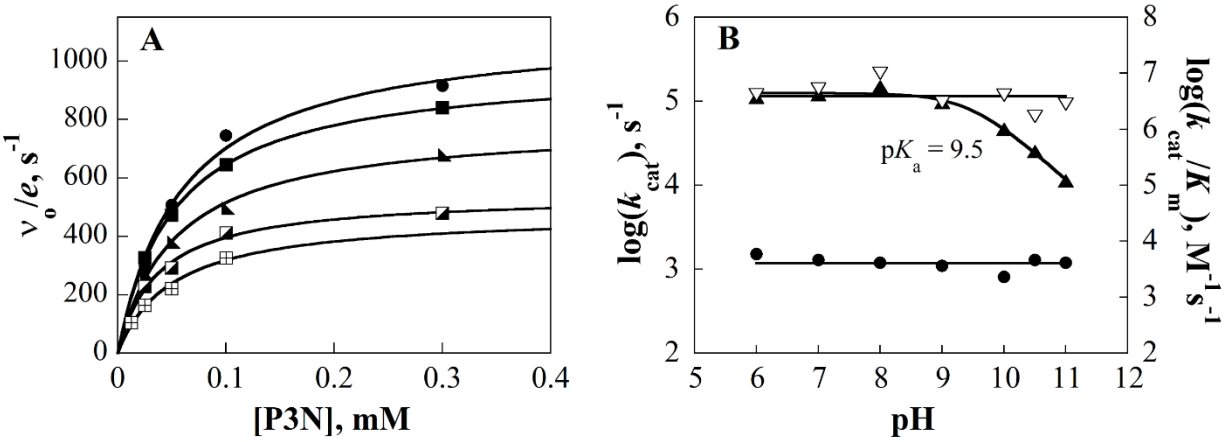


*Figure 2.3 Effect of pH on the steady-state kinetic parameters of wild-type PaNMO. (A) Initial rates of reaction with varying [P3] and [oxygen] determined in 50 mM potassium phosphate, pH 8.0 and 30 °C. [Oxygen] were 28 (⊞), 50 (◪), 88 (◣), 145 (■), and 241 (●) μM. (B) pH-Profiles of the $k_{cat}$ (●), $k_{cat}$ / $K_{P3N}$ (▲), and $k_{cat}$ / $K_{O2}$ (▽) values. Data for the $k_{cat}/K_{P3N}$ value were fit Eq 3.*

### *3.3 pH Effects on the UV-Visible Absorption Spectrum of Wild-Type PaNMO*

The N3 atom of flavin in the oxidized state or the side chain of one of the active site tyrosine residues could be responsible for the p$K_a$ of 9.5 seen in the pH-profile of the $k_{cat}/K_{P3N}$ value. In either case the active site would acquire a negative charge that would hinder binding of the anionic substrate P3N, resulting in a decrease of the $k_{cat}/K_{P3N}$ value. Both ionizations of flavin and tyrosine are associated with large spectral changes in the UV-visible absorption spectrum, with deprotonation of flavin yielding changes at ~490 nm (30,31) and tyrosine at ~300 nm (32,33). Thus, the determination of the pH effects on the UV-visible absorption spectrum of wild-type *Pa*NMO is an effective tool to establish the nature of the group responsible for the pH effect on the observed $k_{cat}/K_{P3N}$ value. As shown in Figure 4A, large spectral changes were seen in the near UV-region of the electromagnetic spectrum of the enzyme when the pH was incrementally raised from 7.8 to 10.4, whereas the visible region of the spectrum was not affected. The maximal spectral changes were centered at 297 nm as seen when the UV-visible absorption spectrum at pH 7.8 was used as a reference and the difference spectra were computed (Figure 4B). A plot of the $\Delta\varepsilon_{297\ nm}$ versus pH yielded a maximal spectral change $\Delta\varepsilon_{297\ nm}$ of 2.4 (±0.1) $M^{-1}cm^{-1}$, consistent with deprotonation of a tyrosine residue (32). A p$K_a$ value of 9.5 (±0.1) could be determined, in perfect agreement with the p$K_a$ value determined kinetically on the $k_{cat}/K_{P3N}$ value.

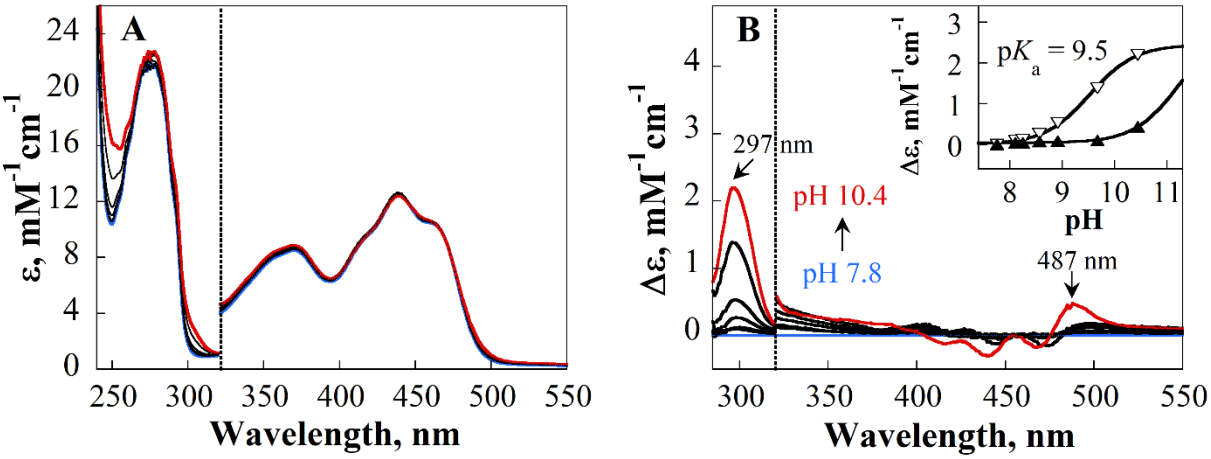


*Figure 2.4 Effect of pH on the UV-visible absorption spectrum of wild-type PaNMO. (A) Enzyme in the range from pH 7.8 (blue) to pH 10.4 (red). (B) Difference UV-visible absorption spectra between the species seen at higher pH values minus the species at pH 7.8. Inset: plot of the Δ297 nm (▽) and Δ487 nm (▲) as a function of the pH; the curves are the fit of the data to Eq 4. The extinction coefficients for the protein absorption band at ≤320 nm were normalized with respect to the flavin absorption bands at ≥320 nm based on the experimentally determined FMN/enzyme stoichiometry of 0.25.*

### *3.4. Steady-state kinetic parameters of PaNMO variant enzymes at pH 8.0*

To characterize the effect of each mutation on substrate binding and catalysis during the oxidation of P3N catalyzed by *Pa*NMO, the steady-state kinetic parameters of the variant enzymes were measured and compared to the wild-type enzyme. To avoid artifactual conclusions stemming from pH effects, pH 8.0 was chosen because the kinetic parameters of the wild-type enzyme determined in this study were pH-independent (Fig. 3B). As for the case of the wild-type enzyme, the best fit of the kinetic data for the Y254F, Y303F, and K307M enzymes was obtained with Eq 2. Small, but not negligible, $K_{ia}$ values

were instead determined with the Y109F and Y299F enzymes (Table 3). With all variant enzymes, the $k_{cat}$ values differed from the wild-type *Pa*NMO by less than 1.5-fold, the $k_{cat}/K_{P3N}$ values by less than 2.5-fold, and the $k_{cat}/K_{O2}$ values by less than 3-fold.

*Table 2.3 Steady-State Kinetic Parameters of Wild-Type and Mutated PaNMO at pH 8.0*

| enzyme | $k_{cat}/K_{P3N}$, $M^{-1}s^{-1}$ | $k_{cat}/K_{O2}$, $M^{-1}s^{-1}$ | $k_{cat}$, $s^{-1}$ | $K_{P3N}$, mM | $K_{O2}$, mM | $K_{ia}$, mM |
|---|---|---|---|---|---|---|
| WT | 5.7 (±0.5) × $10^6$ | 10 (±1) × $10^6$ | 1200 (±100) | 0.21 (±0.01) | 0.12 (±0.01) | - |
| Y109F | 14.0 (±1.0) × $10^6$ | 14 (±1) × $10^6$ | 1400 (±60) | 0.10 (±0.01) | 0.10 (±0.01) | 0.02 (±0.01) |
| Y299F | 8.6 (±0.6) × $10^6$ | 32 (±8) × $10^6$ | 1300 (±20) | 0.15 (±0.01) | 0.04 (±0.01) | 0.10 (±0.02) |
| Y303F | 8.8 (±0.8) × $10^6$ | 14 (±2) × $10^6$ | 970 (±10) | 0.11 (±0.01) | 0.07 (±0.01) | - |
| Y254F | 6.4 (±0.4) × $10^6$ | 26 (±6) × $10^6$ | 1020 (±10) | 0.16 (±0.01) | 0.04 (±0.01) | - |
| K307M | 2.4 (±0.3) × $10^6$ | 13 (±2) × $10^6$ | 1900 (±100) | 0.80 (±0.08) | 0.15 (±0.02) | - |

## 2.5 Discussion

The active site of *Pa*NMO contains a lysine and four tyrosine residues that are fully or highly conserved among ~500 sequences belonging to Class I NMO, suggesting that one or more of these residues may be important for substrate binding or catalysis. The mutagenesis and kinetic study presented here provides evidence demonstrating that the substrate can bind to the active site only when the side chains of the tyrosine residues are in the protonated rather than anionic state, but none of the conserved residues is solely important for substrate binding. Furthermore, the reductive and oxidative half-reactions catalyzed by the enzyme are not affected by the individual substitution of the conserved tyrosine residues with phenylalanine or lysine with methionine, for which evidence is provided below.

The side chains of the tyrosine residues in the active site of *Pa*NMO must be protonated for binding of the negatively charged P3N substrate. Evidence for this conclusion comes from the pH-profiles of the steady-state kinetic parameters and the UV-visible absorption spectrum of the wild-type enzyme. The group with a p$K_a$ value of 9.5 seen in the pH-profile of the $k_{cat}/K_{P3N}$ value must participate in substrate binding because the pH-profile of the $k_{cat}$ value did not show ionization of any group between pH 6.0 and 11.0. This conclusion stems from the fact that while both kinetic parameters report on the kinetic step of flavin reduction from P3N, the $k_{cat}/K_{P3N}$ value also includes the reversible step of substrate binding yielding a Michaelis complex competent for catalysis (34). The participation of a tyrosine residue as being the group responsible for the p$K_a$ of 9.5 comes from the pH-profile of the UV-visible absorption spectrum of the enzyme, showing an increase in absorbance in the 297 nm region of the electromagnetic spectrum that is indicative of the presence of tyrosinate at high pH values. The $\Delta\varepsilon_{297\ nm}$ value of 2.4 $M^{-1}cm^{-1}$ seen in *Pa*NMO is consistent with deprotonation of a single tyrosine residue, as previously established for tyrosine in solution with a $\Delta\varepsilon_{295\ nm}$ value of 2.8 $mM^{-1}cm^{-1}$ and in the active site of a ketosteroid isomerase D40N mutant with a $\Delta\varepsilon_{295\ nm}$ value of 2.6 $mM^{-1}cm^{-1}$ (32). We have made no attempts to determine which tyrosine residue is responsible for the pH effects seen in *Pa*NMO because it is likely that in the confined space of the active site of the enzyme any of the four tyrosine residues would deprotonate at high pH irrespective of which single tyrosine to phenylalanine mutation would be tested. To our knowledge this is the first instance in which deprotonation of an active site tyrosine residue rather than the N3 atom of the oxidized flavin has been reported in a flavin-dependent enzyme. Many flavin-dependent enzymes have one or more tyrosine residues

in the active site (35-40). Because the absorption changes in the near-UV region of the electromagnetic spectrum attributable to tyrosine ionization are small with reference to the strong protein absorbance and the focus is typically on the visible region associated with the flavin, tyrosine ionizations may have been overlooked in previous studies.

The reductive half-reaction in which the enzyme-bound FMN is reduced to the semiquinone state through a single electron transfer from the P3N substrate is not affected by the individual replacement of any of the tyrosine residues with phenylalanine or the lysine with methionine. Evidence to support this conclusion comes from the comparison of the $k_{cat}/K_{P3N}$ values determined with P3N and oxygen as substrates for the wild-type and the mutant enzymes at pH 8.0. With the Y254F, Y299F, Y303F, and K307M, the $k_{cat}/K_{P3N}$ value was ≤2.5-fold than in the wild-type enzyme. In contrast, replacement of Y109 with phenylalanine yielded a 2.5-fold increase in the $k_{cat}/K_{P3N}$ value. When one considers the energetics associated with the changes in the $k_{cat}/K_{P3N}$ value, the mutant enzymes differ from the wild-type by ~0.1 kJ/mol or less, consistent with negligible contributions of the side chains of the lysine and tyrosine residues towards the capture of P3N into an enzyme-substrate complex the proceeds to catalysis. These data, in turn, indicate that none of the conserved lysine or tyrosine residues in the active site of the enzyme are important for either substrate binding or the electron transfer reaction yielding the reduction of the flavin by P3N.

The oxidative half-reaction in which the enzyme-bound FMN is oxidized is not affected by the individual replacement of any of the tyrosine residues with phenylalanine or the lysine with methionine. This conclusion stems from the comparison of the $k_{cat}/K_{O2}$ values determined with P3N and oxygen as substrates for the wild-type and the mutant

enzymes at pH 8.0. With all mutant enzymes the $k_{cat}/K_{O2}$ value is between 1.3- and 3.2-fold larger than in the wild-type enzyme, with values between $1.4 \times 10^7$ $M^{-1}s^{-1}$ and $3.2 \times 10^7$ $M^{-1}s^{-1}$. As for the case of the reductive half-reaction, the corresponding energetic contribution associated with the individual replacement of lysine with methionine or tyrosine with phenylalanine in the active site of the enzyme is negligible, with at the most the electron transfer that results in flavin oxidation being favored by a mere 0.2 kJ/mol in the mutant enzymes as compared to wild-type *Pa*NMO.

In summary, the results presented in this study demonstrate that the tyrosine residues in the active site of *Pa*NMO must be in the protonated form to allow binding of the anionic P3N substrate and catalysis. However, the replacement of any of the four tyrosine residues, i.e., Y109, Y254, Y299, and Y303, with phenylalanine or K307 with methionine does not affect substrate binding or the electron transfer reactions yielding the flavin-mediated oxidation of P3N with oxygen. Thus, the compelling question of why these residues are conserved among ~500 proteins in the active site of Class I NMO remains unattended. One can speculate that because substrate oxidation in NMO does not involve a hydride transfer between NAD(P)H and the enzyme-bound flavin, the geometry and special arrangement of the reactive centers in the enzyme-substrate complex to allow electron transfer from P3N and flavin is less critical than in other flavin-dependent monooxygenases. Thus, having multiple hydroxyl groups in the active site would ensure P3N binding. Alternatively, it is possible that NMO might catalyze other biochemical reactions, besides the very efficient oxidation of P3N, and that the tyrosine and lysine residues have been conserved in the active site due to an unknown selective pressure. This study also offers the first example of a flavin-dependent enzyme in which

tyrosine/tyrosinate equilibrium has been demonstrated spectroscopically in the active site of the enzyme, rather than the classical ionization of the N3 atom of the flavin at high pH values.

## 2.6 References


1. Francis, K., and Gadda, G. (2008) The nonoxidative conversion of nitroethane to ethylnitronate in Neurospora crassa 2-nitropropane dioxygenase is catalyzed by histidine 196. *Biochemistry* **47**, 9136-9144
2. Salvi, F., Agniswamy, J., Yuan, H., Vercammen, K., Pelicaen, R., Cornelis, P., Spain, J. C., Weber, I. T., and Gadda, G. (2014) The combined structural and kinetic characterization of a bacterial nitronate monooxygenase from Pseudomonas aeruginosa PAO1 establishes NMO class I and II. *J Biol Chem* **289**, 23764-23775
3. Smitherman, C., and Gadda, G. (2013) Evidence for a Transient Peroxynitro Acid in the Reaction Catalyzed by Nitronate Monooxygenase with Propionate 3-Nitronate. *Biochemistry* **52**, 2694-2704
4. Agniswamy, J., Reis, R. A. G., Wang, Y. F., Smitherman, C., Su, D., Weber, I., and Gadda, G. (2018) Crystal structure of yeast nitronate monooxygenase from Cyberlindnera saturnus. *Proteins* **86**, 599-605
5. Gorter, K. (1920) Hiptagin, a new glucoside from Hiptage madablota. *Bull. Jard. Bot. Buitenz.* **2**, 187
6. Hipkin, C. R., Simpson, D. J., Wainwright, S. J., and Salem, M. A. (2004) Nitrification by plants that also fix nitrogen. *Nature* **430**, 98
7. Chomcheon, P., Wiyakrutta, S., Sriubolmas, N., Ngamrojanavanich, N., Isarangkul, D., and Kittakoop, P. (2005) 3-Nitropropionic acid (3-NPA), a potent antimycobacterial agent from endophytic fungi: is 3-NPA in some plants produced by endophytes? *J Nat Prod* **68**, 1103-1105
8. Andolfi, A., Boari, A., Evidente, M., Cimmino, A., Vurro, M., Ash, G., and Evidente, A. (2015) Gulypyrones A and B and Phomentrioloxins B and C Produced by Diaporthe gulyae, a Potential Mycoherbicide for Saffron Thistle (Carthamus lanatus). *J Nat Prod* **78**, 623-629
9. Pasteels, J. M., Braekman, J. C., Daloze, D., and Ottinger, R. (1982) Chemical defence in chrysomelid larvae and adults. *Tetrahedron* **38**, 1891-1897
10. Randoux, T., Braekman, J. C., Daloze, D., and Pasteels, J. M. (1991) De novo biosynthesis of Delta(3)-Isoxazolin-5-one and 3-Nitropropanoic acid derivatives inChrysomela tremulae. *Naturwissenschaften* **78**, 313-314
11. Francis, K., Smitherman, C., Nishino, S. F., Spain, J. C., and Gadda, G. (2013) The biochemistry of the metabolic poison propionate 3-nitronate and its conjugate acid, 3-nitropropionate. *IUBMB Life* **65**, 759-768

12. Brouillet, E., Jacquard, C., Bizat, N., and Blum, D. (2005) 3-Nitropropionic acid: a mitochondrial toxin to uncover physiopathological mechanisms underlying striatal degeneration in Huntington's disease. *J Neurochem* **95**, 1521-1540
13. Liu, D. (2019) *Handbook of foodborne diseases*, Taylor & Francis, Boca Raton
14. James, L. F., Hartley, W. J., Williams, M. C., and Van Kampen, K. R. (1980) Field and experimental studies in cattle and sheep poisoned by nitro-bearing Astragalus or their toxins. *American journal of veterinary research* **41**, 377-382
15. Francis, K., Nishino, S. F., Spain, J. C., and Gadda, G. (2012) A novel activity for fungal nitronate monooxygenase: Detoxification of the metabolic inhibitor propionate-3-nitronate. *Arch Biochem and Biophys* **521**, 84-89
16. Francis, K., Russell, B., and Gadda, G. (2005) Involvement of a flavosemiquinone in the enzymatic oxidation of nitroalkanes catalyzed by 2-nitropropane dioxygenase. *J Biol Chem* **280**, 5195-5204
17. Su, D., Kabir, M. P., Orozco-Gonzalez, Y., Gozem, S., and Gadda, G. Fluorescence Properties of Flavin Semiquinone Radicals in Nitronate Monooxygenase. *ChemBioChem* **0**
18. Inoue, H., Nojima, H., and Okayama, H. (1990) High efficiency transformation of Escherichia coli with plasmids. *Gene* **96**, 23-28
19. Bush, M. T., Touster, O., and Brockman, J. E. (1951) The production of beta-nitropropionic acid by a strain of Aspergillus flavus. *J Biol Chem* **188**, 685-693
20. Lewis, R. J. (1996) *Sax's Dangerous Properties of Industrial Materials*, 9th ed., Van Nostrand Reinhold, New York
21. Goodall, D. M., and Long, F. A. (1968) Protonation of nitroalkane anions by acetic acid in mixed water-deuterium oxide solvents. *Journal of the American Chemical Society* **90**, 238-243
22. Nielsen, A. T. (1969) *Nitronic acids and esters. In the Chemistry of the Nitro and Nitroso Groups.* , Intersciene Publishers, New York
23. Aliverti, A., Curti, B., and Vanoni, M. A. (1999) Identifying and quantitating FAD and FMN in simple and in iron-sulfur-containing flavoproteins. *Methods in molecular biology (Clifton, N.J.)* **131**, 9-23
24. Whitby, L. G. (1953) A new method for preparing flavin-adenine dinucleotide. *Biochem J* **54**, 437-442
25. Bradford, M. M. (1976) A rapid and sensitive method for the quantitation of microgram quantities of protein utilizing the principle of protein-dye binding. *Anal Biochem* **72**, 248-254
26. Orozco-Gonzalez, Y., Kabir, M. P., and Gozem, S. (2019) Electrostatic Spectral Tuning Maps for Biological Chromophores. *The Journal of Physical Chemistry B*
27. Su, D., Yuan, H., and Gadda, G. (2017) A Reversible, Charge-Induced Intramolecular C4a-S-Cysteinyl-Flavin in Choline Oxidase Variant S101C. *Biochemistry* **56**, 6677-6690
28. Macheroux, P., Massey, V., Thiele, D. J., and Volokita, M. (1991) Expression of spinach glycolate oxidase in Saccharomyces cerevisiae: purification and characterization. *Biochemistry* **30**, 4612-4619
29. Schwans, J. P., Sunden, F., Gonzalez, A., Tsai, Y., and Herschlag, D. (2013) Uncovering the determinants of a highly perturbed tyrosine pKa in the active site of ketosteroid isomerase. *Biochemistry* **52**, 7840-7855

30. Latovitzki, N., Halper, J. P., and Beychok, S. (1971) Spectrophotometric Titration of Tyrosine Residues in Human Lysozyme. *Journal of Biological Chemistry* **246**, 1457-1460
31. Cleland, W. W. (1963) The kinetics of enzyme-catalyzed reactions with two or more substrates or products: I. Nomenclature and rate equations. *Biochimica et Biophysica Acta (BBA) - Specialized Section on Enzymological Subjects* **67**, 104-137
32. Murray, M. S., Holmes, R. P., and Lowther, W. T. (2008) Active site and loop 4 movements within human glycolate oxidase: implications for substrate specificity and drug design. *Biochemistry* **47**, 2439-2449
33. Wohlfahrt, G., Witt, S., Hendle, J., Schomburg, D., Kalisz, H. M., and Hecht, H.-J. (1999) 1.8 and 1.9 A resolution structures of the Penicillium amagasakiense and Aspergillus niger glucose oxidases as a basis for modelling substrate complexes. *Acta Crystallographica Section D* **55**, 969-977
34. Xia, Z.-x., and Mathews, F. S. (1990) Molecular structure of flavocytochrome b2 at 24 Å resolution. *Journal of Molecular Biology* **212**, 837-863
35. Fu, G., Yuan, H., Li, C., Lu, C. D., Gadda, G., and Weber, I. T. (2010) Conformational changes and substrate recognition in Pseudomonas aeruginosa D-arginine dehydrogenase. *Biochemistry* **49**, 8535-8545
36. Sobrado, P., and Fitzpatrick, P. F. (2003) Identification of Tyr413 as an active site residue in the flavoprotein tryptophan 2-monooxygenase and analysis of its contribution to catalysis. *Biochemistry* **42**, 13833-13838
37. Schreuder, H. A., van der Laan, J. M., Hol, W. G. J., and Drenth, J. (1988) Crystal structure of p-hydroxybenzoate hydroxylase complexed with its reaction product 3,4-dihydroxybenzoate. *Journal of Molecular Biology* **199**, 637-648

# 3 ON THE IMPORTANCE OF H183 IN THE ELECTRON TRANSFER REACTION IN NITRONATE MONOOXYGENASE

## 3.1 Abstract

Propionate 3-nitronate (P3N) is a toxin found in nature that irreversibly inhibits the Krebs cycle – an essential life sustaining metabolic pathway. Nitronate monooxygenase (NMO) is a flavin-dependent enzyme that detoxifies P3N using molecular oxygen ($O_2$). Among ~500 NMO sequences from different organisms, H183 is a fully conserved active site residue in NMO. Kinetic and structural studies were carried out on the H183Q enzyme to investigate the role of H183 in the formation of the ES complex with P3N. The crystal structure of the H183Q enzyme in the presence and absence of substrate analog 3-nitropropionate demonstrated inactive and active conformations of the enzyme active site. In the free H183Q enzyme, the Q183 sidechain blocks the N(5) atom of the flavin leading to an inactive enzyme. Upon substrate binding, an isomerization of the Q183 sidechain accommodates the substrate analog. An extended lag in reaction was observed in the stopped-flow traces of the reduction of the H183Q enzyme with P3N, suggesting an isomerization of the ES complex is required for the single-electron transfer from P3N to the flavin. These results suggest that the side chain of H183 is important for both binding the substrate into an ES complex competent for catalysis and the subsequent single-electron transfer reaction from the nitronate substrate to the flavin.

## 3.2 Introduction

Nitronate monooxygenase (NMO; E.C. 1.13.12.16) from *Pseudomonas aeruginosa* PAO1 (*Pa*NMO) oxidizes toxic, highly reactive nitronates such as propionate 3-nitronate using molecular oxygen ($O_2$). Biochemical studies on *Pa*NMO have demonstrated that the oxidation of P3N with $O_2$ is highly efficient; kinetic studies have shown that P3N is oxidized with oxygen at 102,000,000 $M^{-1}$ $s^{-1}$. Such an impressive rate constant underscores the necessary and rapid oxidation of P3N in living organisms. The physiological substrate of *Pa*NMO is propionate 3-nitronate (P3N) (5). P3N, the conjugate base of 3-nitropropionic acid (3-NPA), is a highly toxic alkyl nitronate that interrupts the Krebs cycle by irreversibly inhibiting succinate dehydrogenase – a vital metabolic enzyme (1,14,41). P3N toxicity has been observed in humans and mammals with symptoms of dystonia, respiratory distress, and foaming of the mouth (2,42). Recently, the hospitalization of a 65-year-old male resulting in death by 3-nitropropionic acid intoxication was reported (43). Over 4,000 genes are currently annotated as putative NMOs from various organisms. Approximately, 500 sequences contain four distinct motifs of NMO coming from bacterial, fungal, and animal sources (5). Among these putative NMOs, several key residues such as Y109, Y303, Y299, H133, and H183 are conserved. H183 is a fully conserved residue located on an active site loop 5.7 Å above FMN. To date, no mutagenesis studies have been conducted on His183.

Similar to His183 in *Pa*NMO, the active sites of glucose-methanol-choline (GMC) oxidoreductases and the L-$\alpha$-hydroxyacid dehydrogenase (LHAD) families contain a histidine positioned ≤5 Å around the N(5) atom of the flavin cofactor (44). Histidines found in the active sites of GMC and LHAD enzyme families have well-characterized

and diverse roles described in recent literature (44). The roles of these histidine residues in the GMC family include alkoxide intermediate stabilization, proton abstraction, stabilization of oxygen radicals, and contribution to the polarity of the active site. H516 in glucose oxidase (GOX) from *Aspergillus niger* is responsible for enhancing the electron transfer from the reduced flavin to molecular oxygen through an electrostatic interaction. In choline oxidase from *Arthrobacter globiformis*, H466 contributes to the active site polarity to allow for proton transfer from the substrate and affects the rate of flavin oxidation by altering the electrophilicity of the reduced flavin (45). The role of orthologous histidines in LHAD enzymes require further work to classify the residue as a catalytic base in this family of enzymes. Crystal structures of a ligand bound in the active site of LHAD enzymes glycolate oxidase (GOX), flavocytochrome $b_2$ (FCB2), and L-lactate 2-monooxygenase (LMO) amongst others have been solved, and it was determined that the ligand is positioned close to the conserved histidine residue and approximately ~4 Å from the N(5) atom of the flavin. In the LHAD enzymes *Ms*LMO and *Sc*FCB2, H290 and H373 residues were mutated to glutamines and the subsequent mutants resulted in reduced activity with their substrate. However, the mutant FCB2 H373Q resulted in a change of position for many surrounding active site residues. In *Hs*GOX, alanine and glutamine mutants resulted in an alteration in the binding pocket such that no flavin was detected in these proteins. The role of conserved histidine residues in GMC and LHAD enzymes demonstrate a major role on the interaction of the enzyme with the substrate and localization of nearby residues.

The active site of *Pa*NMO contains two fully conserved histidine residues proximal to the flavin. H133 is adjacent to the carbonyl on the C(2) locus of FMN and is

a highly conserved residue in putative NMOs. Pointing to the N(5)-FMN atom, H183 is oriented 6 Å away from the *si*-face of the FMN and is fully conserved in putative NMOs. Mutagenesis studies on H133 suggest that the residue is not important for the binding of P3N or the formation of the flavin semiquinone found in the reaction mechanism proceeding substrate binding in *Pa*NMO (4,46). To date, there are no kinetic or crystallographic studies on the involvement of the H183 residue on the detoxification of P3N or the formation of the highly reactive flavin semiquinone intermediate. In NMO from *Neurospora* crassa, H196 is equivalent to H183. H196 acts as a catalytic base which deprotonates and activates its neutral nitroalkane substrate (6). However, in *Pa*NMO, no catalytic base is detected (4,5). Therefore, H183 is more likely involved in binding and orienting the substrate P3N for efficient catalysis.

H183 in *Pa*NMO serves as a good model system for analyzing the role of conserved active site histidine residues in the GMC and LHAD families. GMC and LHAD enzymes and NMOs share a conserved active site histidine located above the isoalloxazine. Based on similarities of substrate binding sites across various flavoproteins, NMO serves as a good model to describe enzyme-substrate interactions outside of base-catalysis for GMC and LHAD enzymes (47). Attempts at characterizing the role of the conserved histidine in GMC and LHAD enzymes has led to understanding its role as a base catalyst. However, these mutagenesis studies do not address the role of the conserved histidine in enzyme-substrate interactions outside of base catalysis. H183 in NMO is a good model system in understanding these enzyme-substrate interactions because it lacks the ability to act as a base, while spatial orientation and substrate and flavin binding sites remain the same.

In this study, the role of H183 at the mechanistic and molecular level is described. H183 was replaced with glutamine and the resulting variant enzyme was purified to high levels. To gain a mechanistic understanding on the role of H183, various steady-state kinetic and rapid-reaction kinetic approaches were used in conjunction with x-ray crystallography. The importance of H183 in substrate capture and orientation and its effect on the single electron transfer to the flavin was investigated.

## 3.3 Results

*Purification and spectral properties of H183Q variant* – To obtain purified recombinant enzyme, the variant H183Q enzyme was purified following the same protocol as the wild-type enzyme (5). The UV-visible absorption spectrum of the H183Q variant enzyme showed the typical spectrum of an oxidized flavoprotein such as wild-type *Pa*NMO with peaks 370 and 441 nm (Figure 3.1). The H183Q variant showed a difference in the absorption intensity and wavelength maxima by at least 1 $mM^{-1}$ $cm^{-1}$ from 300 to 500 nm.

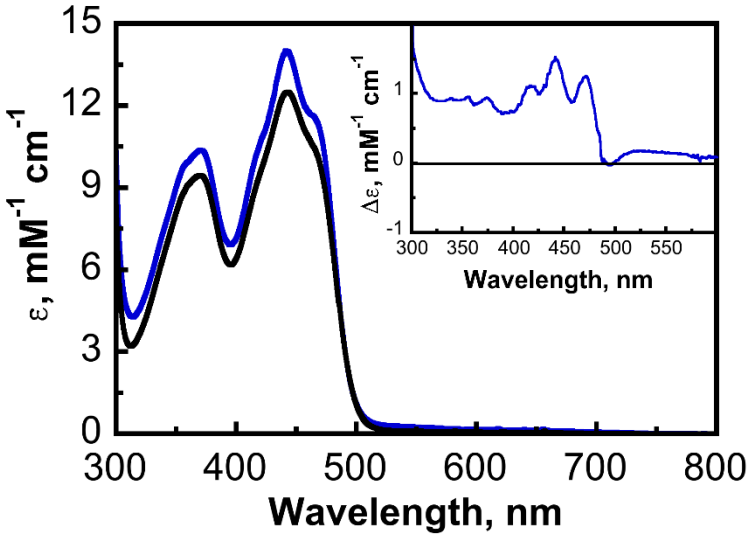


*Figure 3.1 UV−visible absorption spectra of H183Q (blue) and wild-type PaNMO (black). The spectra were recorded in 10 mM Tris-Cl, 10% glycerol at pH 8.0. The inset shows the difference absorption spectra of the enzyme-bound flavin in the H183Q enzyme variant minus the wild-type enzyme.*

*Table 3.1 Steady state kinetic parameters of wild-type and H183Q variant PaNMO.*

| Enzyme | $k_{cat}$, $s^{-1}$ | $k_{cat}/K_{P3N}$, $M^{-1}s^{-1}$ | $k_{cat}/K_{O2}$, $M^{-1}s^{-1}$ | $K_{P3N}$, mM | $K_{O2}$, mM |
|---|---|---|---|---|---|
| H183Q | 30 | 77,000 | 550,000 | 0.40 | 0.10 |
| [B]WT | 1,200 | 5,700,000 | 10,000,000 | 0.21 | 0.12 |

The steady state kinetic parameters were obtained in 50 mM potassium phosphate, pH 8.0 and 30 °C.
[B]Obtained from Ref (14).
Data were fit using Eq. 1.
All values carry a standard error of ≤15%.

*Steady-state kinetics of the H183Q variant* – The steady-state kinetic mechanism for the H183Q variant enzyme was determined at pH 8.0 and 15 °C and 30 °C at varying concentrations of oxygen and P3N. The steady-state kinetic mechanism for the wild-type enzyme had been determined at pH 8.0 and 30 °C, previously (48). Table 3.1

compares the steady-state kinetic rate constants determined for the wild-type and H183Q variant enzyme at 30 °C. The best fits of the data were obtained with Eq.3. As summarized in Table 3.2, the replacement of histidine with a glutamine in the 183 position of NMO resulted in at least a 40-fold decrease in $k_{cat}$ and a 74-fold decrease in $k_{cat}/K_{P3N}$.

In order to compare the steady-state kinetic parameters (e.g. $k_{cat}$, $k_{cat}/K_{P3N}$) to kinetic rate constants for flavin reduction and P3N binding (e.g. $k_{red}$, $k_{red}/K_D$) which were measured in a stopped-flow spectrophotometer, the steady-state kinetics were carried out at 15 °C. Table 3.2 compares the steady-state kinetic parameters to kinetic rate constants for flavin reduction. Values for the turnover number $k_{cat}$ and flavin reduction $k_{red}$ are similar. Additionally, values for the Michaelis constant $K_{P3N}$ and P3N binding $K_D$ are equal to each other within experimental error. Altogether, these observations demonstrate that the $k_{cat}$ and $K_m$ are direct reporters on flavin reduction and substrate binding, respectively.

*Table 3.2 Steady state and rapid kinetic parameters of PaNMO H183Q variant with P3N as substrate.*

| Enzyme | [a]$k_{cat}$, $s^{-1}$ | [b]$k_{red}$, $s^{-1}$ | [a]$K_{P3N}$, mM | [b]$K_d$, mM |
|---|---|---|---|---|
| H183Q | 14.0 ± 0.4 | 12.4 ± 0.2 | 0.17 ± 0.01 | 0.18 ± 0.01 |

[a]The steady state kinetic parameters were obtained in 50 mM potassium phosphate, pH 8.0 and 15 °C.
[b]The rate of flavin reduction $k_{red}$ and the equilibrium constant $K_d$ were measured through a stopped-flow spectrophotometer made anaerobic in 50 mM potassium phosphate at pH 8.0 and 15 °C.

*Kinetic solvent viscosity effects* – The effect of solvent viscosity on the apparent steady state kinetic parameters $k_{cat}$ and $k_{cat}/K_m$ for P3N was evaluated to establish whether substrate binding or product release limits catalysis. These determinations were carried out with glycerol as viscosigen and at pH 8.3. In Figure 3.2, the normalized

$k_{cat}$ and $k_{cat}/K_m$ values determined at increasing relative viscosity of the reaction mixture yielded lines with a slope not significantly different from zero with the exception for the value of $k_{cat}/K_m$ for the wild-type enzyme. As shown in Figure 3.2A, the effect of solvent viscosity on the $k_{cat}$ value was negligible. A slope of zero is consistent with the overall turnover number $k_{cat}$ being fully limited by the chemical step of catalysis (49). As shown in Figure 3.2B, the solvent viscosity has a small effect on the $k_{cat}/K_m$ value for the wild-type enzyme, but for the H183Q variant, the effect is not significantly different from zero. A slope not significantly different from zero is consistent with the capture of substrate being limited fully by the chemical step (49). In this case, the chemical step is fully equal to catalysis. In other words, diffusion processes such as substrate and product association or disassociation are much faster than the chemical step, and the overall reaction is fully limited by this chemical step.

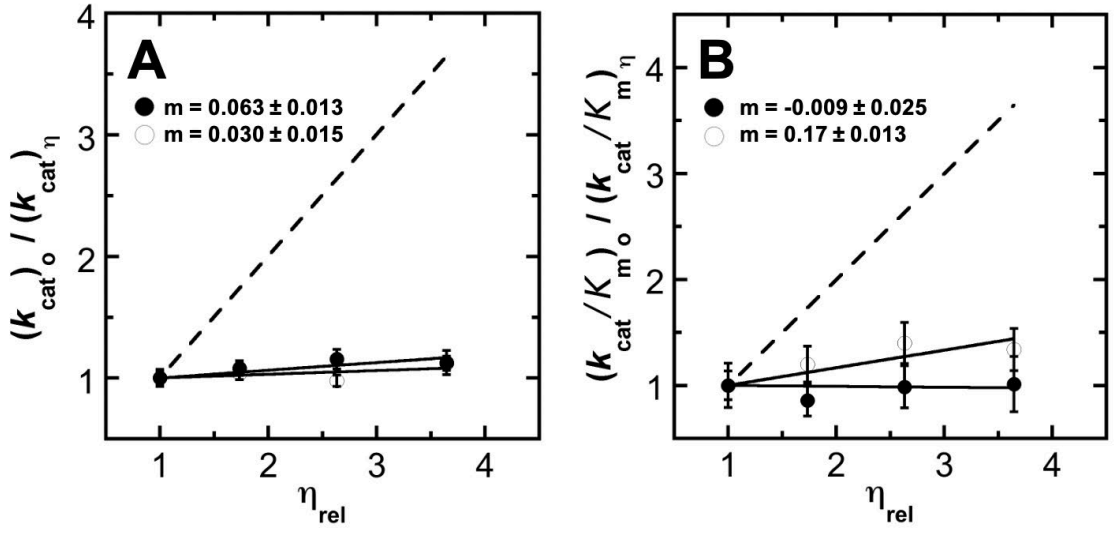


*Figure 3.2 Effect of solvent viscosity on the steady-state kinetic parameters. Panel A: the normalized $k_{cat}$ value for H183Q (●) and wild-type enzymes (○) as a function of relative solvent viscosity with glycerol as microviscogen. Panel B: the normalized $k_{cat}/K_{P3N}$ value for H183Q (●) and wild-type enzymes (○) as a function of relative solvent viscosity with glycerol as microviscogen. All determinations were carried out at 15 °C and pH 8.3.*

*pH-profiles of apparent steady-state kinetics* – The pH dependence of the apparent steady-state kinetic parameters was measured to establish the possible presence of an ionizable group involved in binding or catalysis of the substrate P3N. The initial rates of reaction were determined using an oxygen electrode and by varying the concentration of substrate P3N at 15 $^{o}$C in the pH range of 7.0 to 9.0. pH values below 7.0 were avoided in order to ensure that the substrate P3N would not protonate. The protonation of P3N will result in a neutral molecule and one that does not react with NMO. The apparent steady-state kinetic parameters were calculated using Eq 4 to obtain $k_{cat}$ and $k_{cat}/K_m$ for P3N. In order to ensure an accurate estimation of the $k_{cat}/K_m$ for P3N value, two concentrations of oxygen (atmospheric and 400 μM) at pH extremes 7.0 and 9.0 were tested to establish a saturating concentration of oxygen. As shown in Table 3.3, the H183Q enzyme was pH independent in the tested pH range of 7.0 to 9.0. The H183Q variant enzyme had a maximal $k_{cat}$ value of 8 ± 1 $s^{-1}$ in this pH range.

*Table 3.3 Apparent steady state kinetic rate constants of the PaNMO H183Q variant*

| pH | $k_{cat}$, $s^{-1}$ | $k_{cat}/K_{P3N}$, $M^{-1}s^{-1}$ | $K_{P3N}$, mM |
|---|---|---|---|
| 7 | 8.4 ± 0.1 | 4600 ± 300 | 0.10 ± 0.01 |
| 8 | 6.8 ± 0.3 | 1400 ± 50 | 0.20 ± 0.01 |
| 9 | 8.4 ± 0.3 | 3800 ± 400 | 0.10 ± 0.01 |
| **Average** | **7.9 ± 0.1** | **3300 ± 170** | **0.13 ± 0.06** |

Values were determined at a saturating concentration of the second substrate oxygen.
The steady state kinetic parameters were obtained in 50 mM potassium phosphate and 15 $^{o}$C.
Data were fit using Eq. 2.

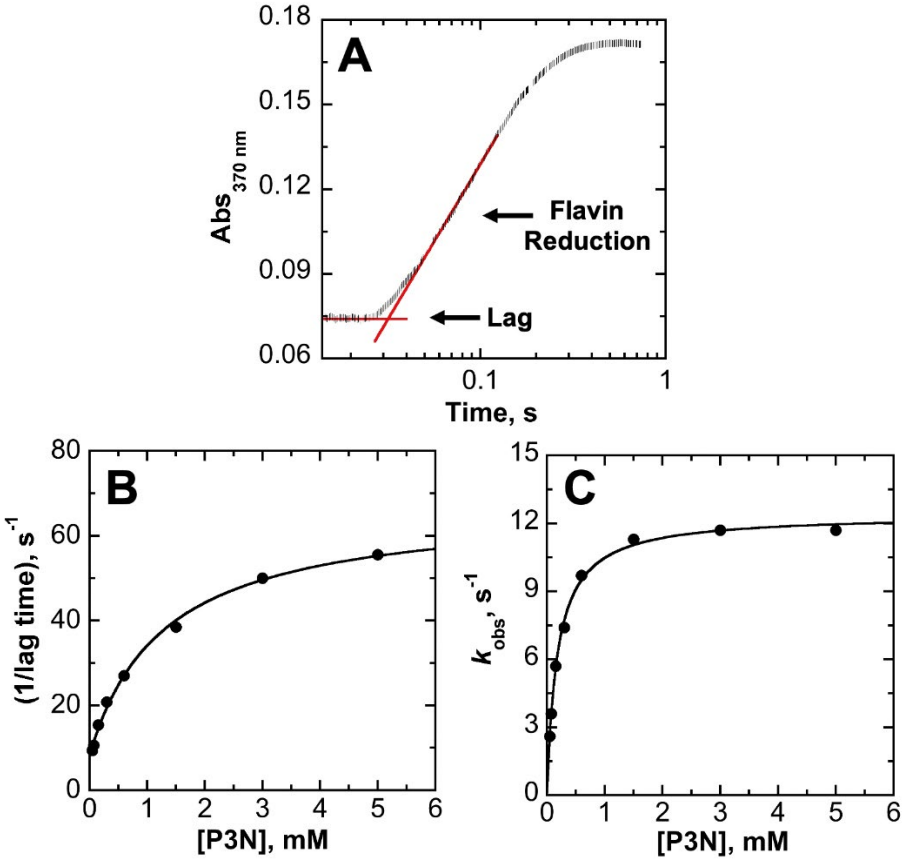


Figure 3.3 Anaerobic reduction of *Pa*NMO H183Q with P3N as substrate in 50 mM sodium phosphate, pH 8.0, 15 °C, in the presence of 10% glycerol. Panel A: selected trace illustrating the intersecting point between the end of the lag period and flavin reduction. Panel B: observed lag times, defined by the intersecting point in panel A, plotted as a function of substrate concentration fit with $A = Be^{-k_{obs}t} + C$.
Panel C: observed rate constants for flavin reduction as a function of substrate concentration fit with $k_{obs} = \frac{k_{red}S}{K_d + S}$.

Scheme 1. A proposed minimal two-step binding mechanism with P3N as substrate.

$$E_{ox} + S \underset{K_1}{\rightleftharpoons} E_{ox}\,S \underset{k_{iso,rev}}{\overset{k_{iso,for}}{\rightleftharpoons}} {}^{*}E_{ox}\,S \xrightarrow{k_{red}} {}^{*}E_{SQ}\,P$$

$E_{ox}$, the oxidized native enzyme.
S, substrate.
*$E_{ox}$S, the ES complex after the isomerization.
*$E_{SQ}$P, the single electron reduced enzyme (semiquinone state) in complex with the product.
$k_{iso,for}$ & $k_{iso,rev}$, the kinetic rate constants describing the isomerization in the forward and reverse directions, respectively.
$k_{red}$, the kinetic rate constant describing the single electron transfer from the P3N substrate to the flavin cofactor.

*Rapid kinetics* – A two-step binding kinetic mechanism (Scheme 1) was used to fit stopped-flow data. To validate the two-step binding kinetic mechanism, stopped-flow data prior to flavin reduction were collected. The length of a lag phase, preceding the exponential increase associated with flavin reduction, was measured. As shown in Figure 3.3A, the lag phase is a flat region with no change in absorbance that precedes flavin reduction. The length of the lag phase was measured up until flavin reduction. The intersecting point between the lag phase and flavin reduction, as shown in Figure 3.3A, is considered the total lag time. In order to have units of $s^{-1}$ and to compare to other first-order kinetic rate constants, the reciprocal of the total lag time was taken. The reciprocal of this total lag time was then plotted against the concentration of P3N used in each stopped-flow trace and fit using Eq. 1 (Fig. 3.3B).

$$\frac{1}{t_{lag}} = \frac{k_{iso,for}\,[S]}{K_1 + [S]} + k_{iso,rev} \qquad (1)$$

Eq. 1 computes kinetic and equilibria constants that represent the first and second steps of the two-step binding reaction in Scheme 1 where $K_1$ is the dissociation constant for the initial equilibrium for the substrate and the enzyme prior to the isomerization, $k_{iso,for}$ and $k_{iso,rev}$ are the rate constants for the isomerization between ES and *ES, S is the concentration of substrate, and $1/t_{lag}$ is the reciprocal of the total lag time (50). Utilizing the kinetic and equilibria constants obtained from Eq. 1, the $K_D$ value of the two-step binding mechanism from Scheme 1 can be calculated using Eq. 2.

$$K_{D,calc} = \frac{K_1 K_{iso}}{1 + K_{iso}} \quad \text{where} \quad K_{iso} = \frac{k_{iso,rev}}{k_{iso,for}} \qquad (2)$$

The $K_D$ value directly obtained experimentally from the reductive half-reaction experiment is compared to the computed $K_{D,Calc}$ for the two-step binding mechanism (Table 3.4). To account for experimental variability and considering that the kinetic parameters of Table 3.4 did not show significant differences at various pH values, the average values between pH 7 and 9 was used for this analysis. An average value of 0.13 ± 0.02 mM was obtained for the $K_{D,Calc}$ which approximated well to the average experimentally determined $K_D$ value of 0.15 ± 0.07 mM. This kinetic analysis is consistent with the two-step binding mechanism of Scheme 1 being a good kinetic model that explains the stopped-flow data with the H183Q enzyme. This kinetic analysis is consistent with the mechanism of Scheme 1 being a good model that explains the results.

*Table 3.4 Kinetic rate and two-step binding and dissociation constants*

| pH | [a]$K_1$, mM | [b]$k_{iso,for}$, $s^{-1}$ | [c]$k_{iso,rev}$, $s^{-1}$ | [d]$k_{red}$, $s^{-1}$ | [e]$K_D$, mM | [f]$K_{D,calc}$, mM |
|---|---|---|---|---|---|---|
| 7 | 1.4 ± 0.6 | 67 ± 13 | 9 ± 1 | 12.6 ± 0.2 | 0.17 ± 0.02 | 0.12 ± 0.02 |
| 7.5 | 1.5 ± 0.2 | 98 ± 4 | 8 ± 1 | 12.6 ± 0.2 | 0.17 ± 0.02 | 0.11 ± 0.02 |
| 8 | 1.2 ± 0.2 | 59 ± 2 | 8 ± 1 | 12.4 ± 0.2 | 0.18 ± 0.01 | 0.14 ± 0.03 |
| 8.5 | 1.6 ± 0.4 | 100 ± 8 | 9 ± 2 | 12.6 ± 0.3 | 0.11 ± 0.01 | 0.13 ± 0.05 |
| 9 | 1.2 ± 0.2 | 68 ± 4 | 9 ± 2 | 11.6 ± 0.3 | 0.11 ± 0.01 | 0.14 ± 0.04 |
| **Average** | **1.4 ± 0.2** | **78 ± 3** | **8.6 ± 0.7** | **12.4 ± 0.1** | **0.15 ± 0.07** | **0.13 ± 0.02** |

[a]$K_1$ is the first dissociation constant between the substrate and the enzyme prior to the isomerization.
[b,c]$k_{iso,for}$ and $k_{iso,rev}$ are the rate constants for the isomerization between ES and *ES.
[d]$k_{red}$ is the limiting first-order rate constant for flavin reduction at saturating concentration of substrate.
[e]The $K_D$ value is the apparent dissociation constant directly obtained experimentally from the reductive half-reaction experiment and is the overall dissociation constant for substrate binding.
[f]Calculated using $K_{D,calc} = \frac{K_1 K_{iso}}{1 + K_{iso}}$ where $K_{iso} = \frac{k_{iso,rev}}{k_{iso,for}}$.

The reductive half-reaction of the H183Q variant was investigated to obtain insights on the binding of the substrate P3N and flavin reduction using a stopped-flow spectrophotometer. The reductive half-reaction of the wild-type enzyme with P3N could not be investigated because flavin reduction was too fast and occurred almost entirely in the mixing time of the stopped-flow instrument (i.e., 2.2 ms). The stopped-flow traces of the reductive half-reaction of the H183Q variant enzyme with P3N were fit with a single-exponential process (Eq. 5). Each rate of flavin reduction obtained from these traces were plotted against the concentration of P3N and fit to Eq. 6. As shown in Figure 3.3C, the observed rate constant for flavin reduction increased hyperbolically with an increasing concentration of P3N. Values for flavin reduction and a $K_D$ for the enzymatic binding of P3N are summarized in Table 3.4. At various pH values, the $k_{red}$ and $K_D$ obtained do not differ significantly. An average value of 12.4 ± 0.1 $s^{-1}$ and 0.15 ± 0.07 mM was obtained for the $k_{red}$ and $K_D$, respectively, from pH 7.0 to 9.0.

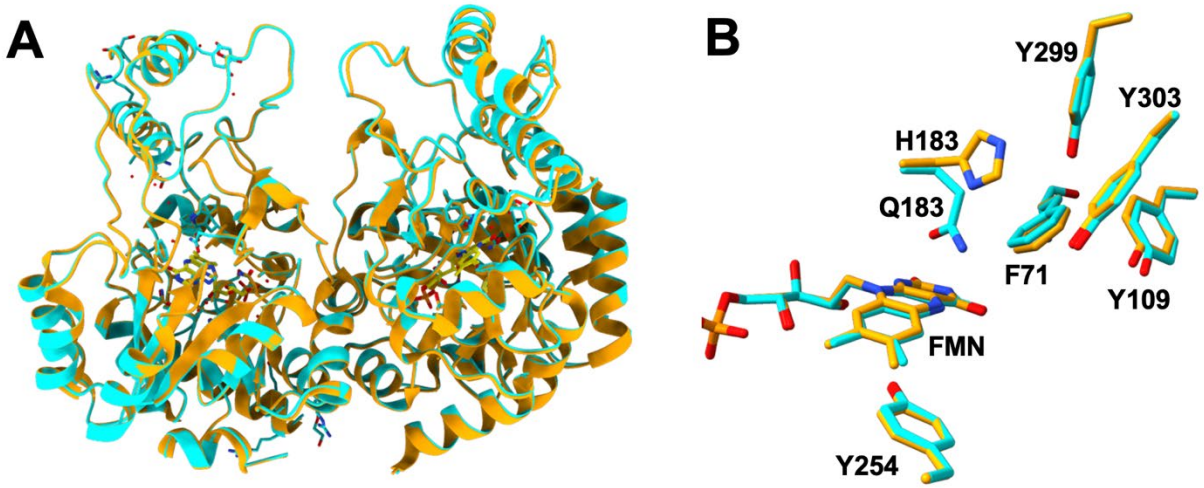


Figure 3.4 Comparison of crystal structures of the H183Q variant and wild-type enzymes of *Pa*NMO. The residues and ribbons represented in orange represent the wild-type *Pa*NMO enzyme, whereas the residues and ribbons in cyan represent the H183Q *Pa*NMO enzyme. Panel A illustrates the overlay between the H183Q variant (cyan) and wild-type (orange) enzymes. Panel B depicts the superposition of the H183Q and wild-type enzyme active sites.

*Overall structure of H183Q variant* – The H183Q variant enzyme and H183Q in complex with the substrate analogue 3-nitropropionate (3-NPA) were crystallized in the monoclinic space group $P2_1$ with two molecules per asymmetric unit. The $R_{work}$ and $R_{free}$ values were 16.2% and 19.1%, respectively, for the partially refined structure of H183Q and 17.5% and 19.8%, respectively, for the partially refined structure of H183Q in complex with 3NPA. The data collection and refinement statistics are reported in Table 3.5. The overall structure of *Pa*NMO H183Q and H183Q-3NPA closely resembled that of PaNMO-WT (PDB 4Q4K), with RMSD values ≤ 0.20 Å for 351 Cα atoms (Figure 3.4) (5). Therefore, the overall fold of the enzyme was not altered by the replacement of histidine to a glutamine in the 183 position. As previously reported for *Pa*NMO, the

protein folded into an FMN-binding domain (residues 1–71, 112–249, and 333–351) and a substrate-binding domain (residues 72–111 and 250–332) (5).

*Table 3.5 X-ray Diffraction Data Collection and Refinement Statistics*

| **Data Collection** | **H183Q *Pa*NMO** | **H183Q *Pa*NMO-3NPA** |
|---|---|---|
| Wavelength (Å) | 1.1 | 1.1 |
| Space group | $P2_1$ | $P2_1$ |
| Unit cell parameters (Å, deg) | a = 69.88, b = 54.25, c=88.29, β = 96.1 | a = 70.00, b = 54.36.4; c=88.64, β = 95.87 |
| Number of molecules per asymmetric unit | 2 | 2 |
| Resolution range (Å) | 42.76 – 1.70 (1.76-1.70)[a] | 39.53 – 1.73 (1.79-1.73)[a] |
| Total observations | 133256 | 127965 |
| Unique reflections | 70207 | 67713 |
| Completeness (%) | 96.55 (96.50) | 97.40 (97.31) |
| $\langle I/\sigma(I) \rangle$ | 9.93 (2.79) | 9.04 (2.2) |
| $R_{merge}$ (%) | 3.1 (23.7) | 3.7 (34.5) |
| Wilson B-factor (Å$^2$) | 19.5 | 21.6 |
| **Refinement** | | |
| $R_{work}$ (%) | 16.2 | 17.5 |
| $R_{free}$ (%) | 19.1 | 19.8 |
| RMS deviations from ideality | | |
| Bond lengths (Å) | 0.016 | 0.012 |
| Angles (°) | 1.85 | 1.43 |
| Number of atoms | | |
| Protein | 5492 | 5436 |
| Water | 524 | 552 |
| Average B-factor (Å$^2$) | | |
| Protein | 24.30 | 26.77 |
| Water | 33.47 | 36.10 |
| Ligands | 24.36 | 35.37 |
| **Ramachandran analyses** | | |
| Outliers (%) | 0 | 0 |
| Favored regions (%) | 97.70 | 97.84 |
| Allowed regions (%) | 2.30 | 2.16 |

[a]Values in parentheses are given for the highest resolution shell.

## 3.4 Discussion

This study reports on the characterization of an active site residue H183 in nitronate monooxygenase from *Pseudomonas aeruginosa* PAO1 (*Pa*NMO). The biochemical and structural investigations here demonstrate that H183 is necessary in arranging the substrate to be in a configuration competent for its electron transfer to the flavin. The crystal structures of a H183Q variant in the presence and absence of the substrate analog demonstrate two conformations for the Q183 side chain i.e., the inactive conformation blocks the reactive center of the flavin and the active conformation arranges the substrate-analog in front of the flavin. These two conformations were observed kinetically using rapid reaction kinetics on a stopped-flow spectrophotometer. The inactive conformation caused a lag in which flavin reduction was delayed due to the Q183 sidechain blocking the flavin. Then, an isomerization produces the active conformation where an exponential increase in absorbance is observed i.e., the flavin becomes reduced by a single electron. These data altogether suggest that H183 is important in optimizing the position of the substrate in the active site and the single electron transfer to the flavin.

The electron transfer from P3N to the flavin is fully rate limiting in the H183Q variant enzyme. Evidence in support of this conclusion comes from the steady-state and rapid kinetic measurements of the reaction between the H183Q enzyme and P3N (Table 3.2). The kinetic rate constants $k_{cat}$ and $k_{red}$ are similar to each other thus report directly on the electron transfer from P3N to the flavin in the H183Q enzyme. In the wildtype enzyme, the rate of flavin reduction is too fast to be measured at 15 $^{o}$C which does not allow any insights on the electron transfer. However, additional evidence in support of this conclusion comes from the solvent kinetic viscosity effect experiment where the viscosity of the solution and [P3N] were varied at a saturating concentration of the second substrate oxygen. For both the wildtype and H183Q variant NMOs, the effect of solvent viscosity on $k_{cat}$ was approximately zero which is consistent with the overall turnover number $k_{cat}$ being limited by the electron transfer from P3N to the flavin (Figure 3.2A). In the case where the slope in a viscosity effect plot results in zero, the chemical step in the enzymatic reaction is fully rate limiting (49). Altogether, these data suggest that the electron transfer from P3N to the flavin is fully rate limiting.

H183 plays a major role in the catalytic step and its effect on substrate binding is minimal in *Pa*NMO. Evidence in support of this conclusion comes from the 40-fold decrease in $k_{cat}$ and 74-fold decrease in $k_{cat}/K_{P3N}$ observed in the H183Q variant enzyme (Table 3.1). The kinetic parameters $k_{cat}$ and $k_{cat}/K_{P3N}$ report on the catalytic step i.e. the electron transfer from P3N to the flavin. However, $k_{cat}/K_{P3N}$ includes the substrate binding step which is described by $K_{P3N}$ (51). Thus, $k_{cat}/K_{P3N}$ holds a 40-fold decrease in value and an additional ~2-fold decrease contributed by $K_{P3N}$ i.e. multiplying 40 by 2 approximately equates to the observed 74-fold decrease in $k_{cat}/K_{P3N}$. To summarize, the majority of the 74-fold decrease in $k_{cat}/K_{P3N}$ is mainly contributed by the catalytic step with a small ~2-fold contribution by steps involving substrate binding.

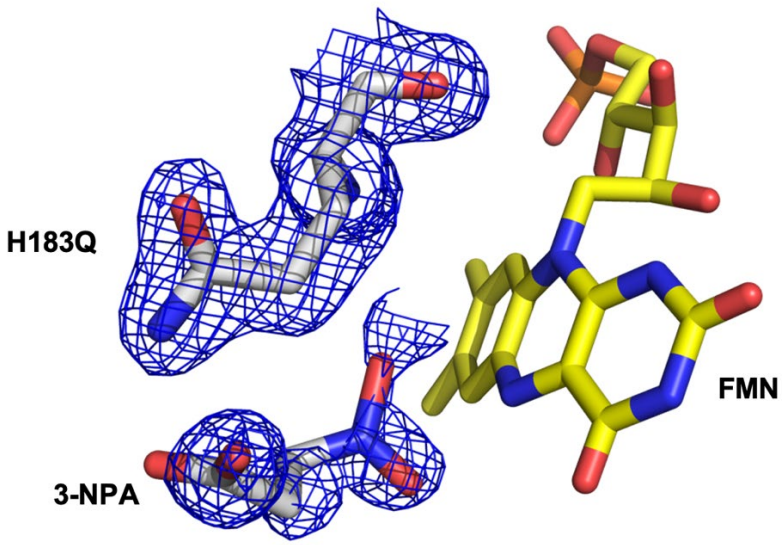


*Figure 3.5 Active site of PaNMO-H183Q variant in complex with substrate analog 3-nitropropionate (3-NPA). The electron density ($2F_o - F_c$ contoured at 1.0σ) is shown for the Q183 variant sidechain and the substrate analog.*

The crystal structure of the H183 variant in complex with the substrate analog represents an electron transfer ready configuration. Evidence for this conclusion comes from the crystal structure of the H183Q variant enzyme in complex with substrate analog 3-nitropropionate (Figure 3.5). The nitro group of the substrate analog is positioned approximately 3.5 Å away from the N(5) atom of the flavin. It is likely that the position of the substrate analog is a good representation of the positioning of P3N prior to its electron transfer to the flavin. Similarly, many flavin dependent enzymes position and oxidize substrates in front of the N(5) atom of the flavin. Fraaije and Mattevi have examined the crystal structures of various flavin-dependent enzymes in complex with their physiological substrates (47). Their examination led to the conclusion that the site of substrate oxidation is found 3.5 Å from the N(5) atom of the flavin. In addition to distances, the site of substrate oxidation had a defining angle with the N(5)-N(10) atoms of 96-117$^{o}$ (47). In this current study, the nitro group of the substrate analog is approximately 122$^{o}$ with reference to the N(5)-N(10) atoms of the flavin. This measurement is in good agreement with the range described in Fraaije and Mattevi's study, especially when taking into account that the crystal structure is a snapshot view of enzyme-substrate dynamic interactions (52).

The H183Q variant binds P3N in a two-step binding process where P3N is bound then the Q183 sidechain switches from inactive to active conformations (Scheme 1). Evidence for this conclusion comes from the fitting of the stopped-flow lag data (Figure 3.3A and 3.3B). The extended lag observed in the stopped-flow traces is inversely dependent on the concentration of P3N. An equation for a two-step binding process (Eq 1) is used to fit these lag data which suggests an isomerization of the ES complex is required for the electron transfer reaction between the substrate and the flavin. In the two-step binding process, the first step is substrate capture i.e., the enzyme binds P3N with equilibrium constant $K_1$. The second step is a conformational change in which the Q183 residue switches from an inactive to active conformation thus positioning P3N for its reaction with the flavin cofactor i.e., a process represented by $k_{iso,for}$ and $k_{iso,rev}$. Using the value of $K_1$ and the ratio of ($k_{iso,rev}$ / $k_{iso,for}$), an overall thermodynamic $K_D$ can be calculated using Eq. 2. This $K_D$ is related to the overall substrate binding process i.e., steps one and two described previously. This overall $K_D$ is also obtained experimentally from the reductive half-reaction experiment (Figure 3.3C) where [P3N] was varied as a function of the observed rate of flavin reduction. To further validate that the H183Q variant enzyme follows this two-step binding model, a self-check is possible by comparing the calculated overall $K_D$ with the one determined experimentally. To summarize these results, Table 3.4 reports the averages of all equilibria and rate constants in addition to the calculated and experimental $K_D$. The average values found in Table 3.4 provide support for the two-step mechanism described in Scheme 1.

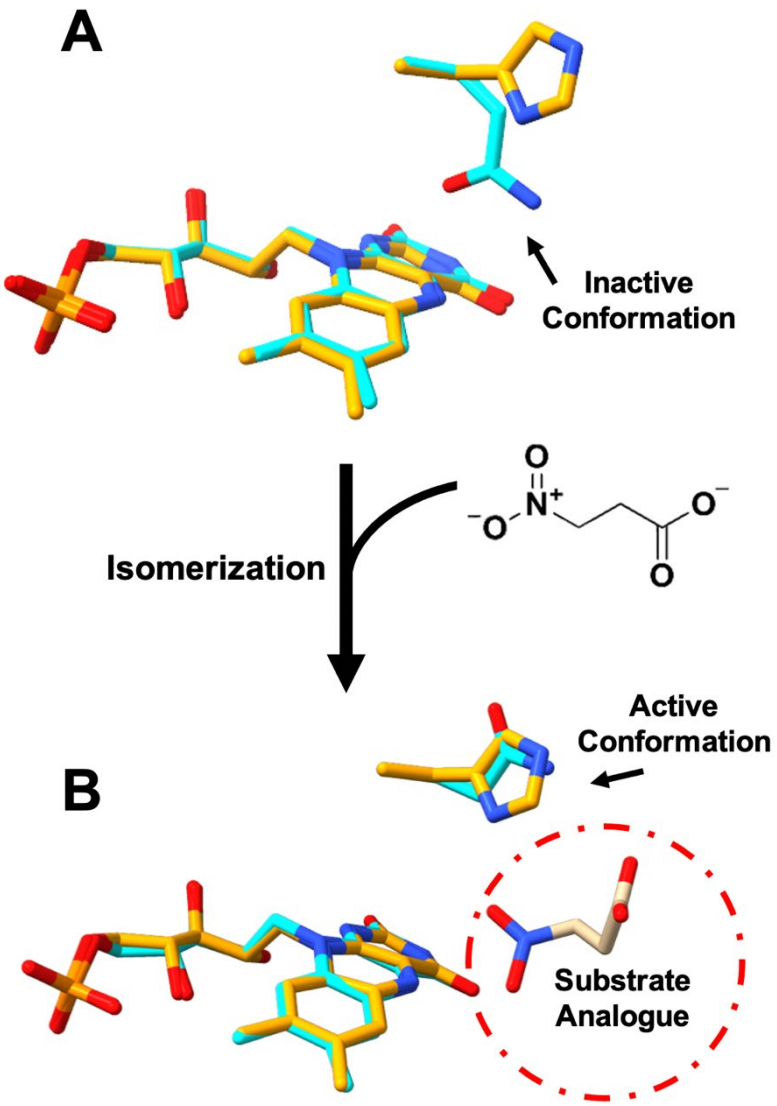


Figure 3.6 Comparison of the crystal structures of the free and bound H183Q variant enzymes to the wild-type *Pa*NMO enzyme. Panel A illustrates an overlay of the variant H183Q (cyan) and wild-type (orange) *Pa*NMO enzymes. The free H183Q variant enzyme occupies an inactive conformation where access to the area in front of the N(5) atom of the flavin is occupied by the 183 side chain. Panel B displays an overlay of the substrate analogue-H183Q variant complex (cyan) and the wild-type (orange) *Pa*NMO enzyme. The Q183 sidechain in H183Q variant enzyme, in complex with a substrate analogue 3-nitropropanoate, occupies an active conformation allowing space in front of the flavin.

H183 is an essential residue in the active site of *Pa*NMO that maintains an active conformation that gates the single-electron transfer from the substrate to the flavin. Evidence for this conclusion comes from the crystal structure of the H183Q variant in the free form and in complex with a substrate analog (Figure 3.6). The H183Q variant enzyme was crystallized in the presence and absence of 3-nitropropionate which is an analog of the physiological substrate P3N. In the crystal structure of the H183Q variant in the free form, the glutamine sidechain is positioned in an inactive conformation and blocks the N(5) atom of the flavin which consequently obstructs the substrate analog from being properly positioned in the active site. However, in the presence of the substrate analog, the glutamine sidechain is positioned in an active conformation and the substrate analog is positioned in front of the N(5) atom of the flavin. Based on the orientation of substrate in numerous flavin-dependent enzymes, the substrate is oxidized after being properly positioned in front of the N(5) atom of the flavin (47). As a result, in the H183Q mutant, the switching from inactive to active conformations gates the single-electron transfer to the flavin.

In conclusion, the kinetic and structural studies done on the H183Q variant from *Pa*NMO has established the role of H183 in the active site of the enzyme. H183 is essential in maintaining an active conformation in the ES complex necessary for the single electron transfer reaction from the P3N substrate to the flavin cofactor. Upon replacement of H183 with a glutamine, the variant enzyme demonstrates to have inactive and active conformations. The mutant Q183 sidechain in the inactive conformation blocks the reactive center of the flavin, while the substrate analog is oriented in front of the reactive center of the flavin in the active conformation. The two

conformations were modeled kinetically using rapid reaction kinetics. An extended lag that is inversely dependent on the concentration of P3N is observed in the stopped-flow traces for the H183Q variant enzyme prior to flavin reduction, suggesting the presence of an isomerization between the inactive and active conformations required for the electron transfer reaction.

## 3.5 Materials and Methods

*Materials* – *Escherichia coli* strains DH5$\alpha$ and Rosetta(DE3)pLysS were from Invitrogen Life Technologies (Grand Island, NY) and Novagen (Madison, WI). The QIAprep Spin Miniprep kit were from Qiagen (Valencia, CA). The oligonucleotides containing the point mutation were from Sigma (The Woodlands, TX). The endonuclease *DpnI* was from New England BioLabs (Ipswich, MA). The HiTrap™ Chelating HP 5 mL affinity column and PD-10 desalting column was from GE Healthcare (Piscataway, NJ). 3-nitropropionate was from Sigma (Milwaukee, WI).

*Site-directed mutagenesis and purification of wild-type and variant enzymes* – The mutant gene for nitronate monooxygenase variant H183F was prepared using the pET20b(+) plasmid harboring the wild-type gene PA4202 as a template The construct containing the correct mutation and sequence was used to transform *E. coli* strain Rosetta(DE3)pLysS competent cells for protein expression. Protein expression and purification were carried out as previously described (5).

*Protein production* – The mutant gene for nitronate monooxygenase variant H183Q was prepared using the pET20b(+) plasmid harboring the wild-type gene PA4202 as a template. The construct containing the correct mutation and sequence was used to transform *E. coli* strain Rosetta(DE3)pLysS competent cells for protein expression. Protein expression and purification were carried out as previously described (5).

*Spectroscopic studies* – The protein concentration was determined using the Bradford method and bovine serum albumin as standard (28). The extinction coefficient of the variant enzyme *Pa*NMO-H183F was determined by heat denaturation. The purified enzyme was passed through a PD-10 desalting column equilibrated with 50 mM potassium phosphate, pH 7.0, before subject to heat denaturation at 100 °C for 30 or 40 min. The denatured protein was removed by centrifugation, and the concentration of unbound FMN was measured by using a molar extinction coefficient at 450 nm of 12,200 $M^{-1}cm^{-1}$ for free FMN (27). An Agilent Technologies diode-array spectrophotometer Model HP 8453 PC was used for these measurements.

*Crystallization* – The variant enzyme H183Q was passed through a PD-10 column equilibrated with 50 mM Tris-Cl, 100 mM NaCl, pH 8.0, and concentrated to 2 mg $mL^{-1}$The enzyme concentration was estimated using the experimental molar extinction coefficient for enzyme-bound FMN. Yellow crystals were grown in the presence of 20% PEG 3350 and 0.1 M Na-HEPES at pH 7.0 within 7 days. The H183Q enzyme was incubated in the presence of 1 mM 3-nitropropionic acid for two hours over

ice under the same conditions. Crystals were grown at room temperature in hanging drops in 2:2 μL enzyme to reservoir solution over 1,000 μL of reservoir solution.

*Data collection and processing* – The crystals were cryo-cooled in the mother liquor with 25% (v/v) glycerol and flash-frozen immediately in liquid nitrogen. X-ray diffraction data were collected at 100K on beamline 22-ID with detector Eiger 16 M of the Southeast Regional Collaborative Access Team (SER-CAT) at the Advanced Photon Source, Argonne National Laboratory. For the H183Q crystal, seven hundred twenty images were collected, at 0.25°oscillation per image. For the H183Q-3NPA crystal, three hundred sixty images were collected, at 0.5°oscillation per image. In both cases, the images were collected with a 200 mm crystal-to-detector distance and an exposure time of 0.25 s per image. Data integration and analysis were carried out using iMOSFLM (53) and AIMLESS (54) in the CCP4 suite (55).

*Structure solution and refinement* – The coordinates of wild-type *Pa*NMO (PDB ID: 4Q4K) (5) were used for the molecular replacement to obtain the initial phases for the H183Q variant. A unique solution was found by *Phaser* in the space group $P2_1$ with two molecules in the asymmetric unit. The structure was refined using *phenix.refine* (56), with manual map inspection and model building being performed in Coot. All structural figures were produced using PyMol (www.pymol.org).

*Enzymatic assays* – The protein concentration was determined using the Bradford method and bovine serum albumin as standard (28). The extinction coefficient of the variant enzyme *Pa*NMO-H183F was determined by heat denaturation. The purified

enzyme was passed through a PD-10 desalting column equilibrated with 50 mM potassium phosphate, pH 7.0, before subject to heat denaturation at 100 °C for 30 or 40 min. The denatured protein was removed by centrifugation, and the concentration of unbound FMN was measured by using a molar extinction coefficient at 450 nm of 12,200 $M^{-1}cm^{-1}$ for free FMN (27). An Agilent Technologies diode-array spectrophotometer Model HP 8453 PC was used for these measurements.

*Steady-state kinetics of the variant H183Q enzyme* – The enzymatic activity of the variant *Pa*NMO *H183Q* enzyme was measured by the method of initial rates of oxygen consumption with a computer-interfaced Oxy-32 oxygen monitoring system (Hansatech Instruments, Inc., Norfolk, England). The steady-state kinetic experiment was performed at 15 or 30 °C in 50 mM potassium phosphate pH 8.0. P3N stocks were prepared as previously described (4). The enzyme concentration of the H183Q enzyme was 0.2 μM, the P3N concentration ranged from 0.50 to 5 mM, and the oxygen concentration ranged from 17 to 111 μM. The reaction mixture was equilibrated to a specific oxygen concentration by bubbling an $O_2/N_2$ gas mixture for at least 5 min. The reaction was initiated with the addition of enzyme then substrate into the reaction mixture. Additionally, the apparent steady-state kinetic parameters of the H183Q enzyme were measured as a function of pH at 15 ºC. This experiment was conducted using the same protocol as the steady-state kinetic assay described above with the exception that the initial rates of reaction were measured at atmospheric $O_2$. A concentration of 400 μM $O_2$ was tested at pH extremes 6 and 9.5 of the pH profile to

ensure that oxygen was at a saturating concentration. This was done to ensure an accurate estimation of the $^{app}(k_{cat}/K_m)$ for P3N.

*Reductive half-reaction* – The reductive half-reaction of the H183Q variant enzyme with P3N was carried out anaerobically with a Hi-Tech SF-61 stopped-flow spectrophotometer (TgK Scientific, United Kingdom). The instrument was made anaerobic by an overnight incubation with 5 mM glucose and 1 μM glucose oxidase in sodium phosphate pH 6.0. The variant enzyme was prepared by passing it through a PD-10 desalting column equilibrated with the corresponding buffer for each pH point. The enzyme sample was transferred to a glass tonometer where it was flushed with ultrapure argon then vacuumed for 20 cycles. P3N stocks were prepared as previously described, placed in syringes, and flushed with ultrapure argon for 25 min. The P3N stocks contained 5 mM glucose and 0.5 μM glucose oxidase in order to ensure removal of oxygen. The concentration of enzyme after mixing was 10 μM and the concentration range of P3N used was 0.050 to 5 mM.

*Kinetic Solvent Viscosity Effects* – The effect of viscosity on the steady-state kinetic parameters for the wild-type and H183Q *Pa*NMO enzymes was determined with glycerol as viscosigen. Enzymatic assays were carried out in the presence of 50 mM sodium pyrophosphate at pH 8.3 and 15 $^{o}$C. Reaction mixtures contained varying amounts of glycerol (0–40%, m/m, η =1.0–3.5 cP). The relative viscosity of the solvent at 15 $^{o}$C was calculated from published values at 20 $^{o}$C (57). Reaction mixtures were

equilibrated at atmospheric oxygen for at least 5 min before the reaction was initiated by addition of the substrate P3N and the enzyme.

*Data analysis* – The kinetic data for the steady-state kinetic experiment where both P3N and $O_2$ were fit to Eq 3. Eq 3 is for a sequential steady-state kinetic mechanism where $v_o$ is the initial velocity of reaction, $e$ is the concentration of enzyme, $k_{cat}$ is a first order rate constant for the turnover of enzyme at saturating concentrations of P3N and $O_2$. The Michalis constants are represented by $K_{P3N}$ and $K_{O2}$. For the apparent steady-state kinetic experiment, the initial rates of reaction were plotted using Eq 4 where $v_o$ is the initial velocity of the reaction at any given concentration of substrate ([S]), $e$ is the concentration of enzyme, $k_{cat}$ is the overall enzyme turnover at saturating substrate concentration, and $K_m$ is the Michaelis constant.

$$\frac{v_o}{e} = \frac{k_{cat}\,[P3N][O_2]}{K_{P3N}[O_2] + K_{O2}[P3N] + [P3N][O_2]} \qquad (3)$$

$$\frac{v_o}{e} = \frac{k_{cat}\,[S]}{K_m + [S]} \qquad (4)$$

Stopped flow traces for the reductive half-reaction were fit with Eq 5 which describes a single exponential process. The observed absorbance changes associated with flavin reduction is described by $k_{obs}$. The absorbance at 372 nm is described by A, the amplitude of absorbance change associated with $k_{obs}$ is B, the absorbance at infinite time is C, and t is time. $k_{obs}$ was plotted as a function of the concentration of substrate

using Eq 6, where $k_{red}$ is the limiting first-order rate constant for flavin reduction at saturating concentration of substrate, $K_D$ is the apparent dissociation constant for substrate binding, and S is the substrate concentration.

$$A = Be^{-k_{obs}t} + C \quad (5)$$

$$k_{obs} = \frac{k_{red}S}{K_d + S} \quad (6)$$

The effects of solvent viscosity on $^{app}k_{cat}$ and $^{app}(k_{cat}/K_m)$ for P3N at saturating oxygen were fit to Eq 7, where $(k)_o$ and $(k)_\eta$ are the kinetic parameters of interested in the absence and presence of viscogen, respectively, S is the degree of dependence of viscosity of the relative kinetic parameter, and $\eta_{rel}$ is the relative viscosity of the reaction solution.

$$\frac{k_o}{k_\eta} = m(\eta_{rel} - 1) + 1 \quad (7)$$

## 3.6 References


1. Coles, C. J., Edmondson, D. E., and Singer, T. P. (1979) Inactivation of succinate dehydrogenase by 3-nitropropionate. *J Biol Chem* **254**, 5161-5167
2. Francis, K., Nishino, S. F., Spain, J. C., and Gadda, G. (2012) A novel activity for fungal nitronate monooxygenase: detoxification of the metabolic inhibitor propionate-3-nitronate. *Arch Biochem Biophys* **521**, 84-89
3. Huijbers, M. M. E., Montersino, S., Westphal, A. H., Tischler, D., and van Berkel, W. J. H. (2014) Flavin dependent monooxygenases. *Archives of Biochemistry and Biophysics* **544**, 2-17
4. Smitherman, C., and Gadda, G. (2013) Evidence for a Transient Peroxynitro Acid in the Reaction Catalyzed by Nitronate Monooxygenase with Propionate 3-Nitronate. *Biochemistry* **52**, 2694-2704
5. Salvi, F., Agniswamy, J., Yuan, H., Vercammen, K., Pelicaen, R., Cornelis, P., Spain, J. C., Weber, I. T., and Gadda, G. (2014) The combined structural and kinetic characterization of a bacterial nitronate monooxygenase from Pseudomonas aeruginosa PAO1 establishes NMO class I and II. *J Biol Chem* **289**, 23764-23775
6. Francis, K., and Gadda, G. (2008) The nonoxidative conversion of nitroethane to ethylnitronate in Neurospora crassa 2-nitropropane dioxygenase is catalyzed by histidine 196. *Biochemistry* **47**, 9136-9144
7. Agniswamy, J., Reis, R. A. G., Wang, Y. F., Smitherman, C., Su, D., Weber, I., and Gadda, G. (2018) Crystal structure of yeast nitronate monooxygenase from Cyberlindnera saturnus. *Proteins* **86**, 599-605
8. Gorter, K. (1920) Hiptagin, a new glucoside from Hiptage madablota. *Bull. Jard. Bot. Buitenz.* **2**, 187
9. Hipkin, C. R., Simpson, D. J., Wainwright, S. J., and Salem, M. A. (2004) Nitrification by plants that also fix nitrogen. *Nature* **430**, 98
10. Chomcheon, P., Wiyakrutta, S., Sriubolmas, N., Ngamrojanavanich, N., Isarangkul, D., and Kittakoop, P. (2005) 3-Nitropropionic acid (3-NPA), a potent antimycobacterial agent from endophytic fungi: is 3-NPA in some plants produced by endophytes? *J Nat Prod* **68**, 1103-1105
11. Andolfi, A., Boari, A., Evidente, M., Cimmino, A., Vurro, M., Ash, G., and Evidente, A. (2015) Gulypyrones A and B and Phomentrioloxins B and C Produced by Diaporthe gulyae, a Potential Mycoherbicide for Saffron Thistle (Carthamus lanatus). *J Nat Prod* **78**, 623-629
12. Pasteels, J. M., Braekman, J. C., Daloze, D., and Ottinger, R. (1982) Chemical defence in chrysomelid larvae and adults. *Tetrahedron* **38**, 1891-1897
13. Randoux, T., Braekman, J. C., Daloze, D., and Pasteels, J. M. (1991) De novo biosynthesis of Delta(3)-Isoxazolin-5-one and 3-Nitropropanoic acid derivatives inChrysomela tremulae. *Naturwissenschaften* **78**, 313-314
14. Francis, K., Smitherman, C., Nishino, S. F., Spain, J. C., and Gadda, G. (2013) The biochemistry of the metabolic poison propionate 3-nitronate and its conjugate acid, 3-nitropropionate. *IUBMB Life* **65**, 759-768

15. Brouillet, E., Jacquard, C., Bizat, N., and Blum, D. (2005) 3-Nitropropionic acid: a mitochondrial toxin to uncover physiopathological mechanisms underlying striatal degeneration in Huntington's disease. *J Neurochem* **95**, 1521-1540
16. Liu, D. (2019) *Handbook of foodborne diseases*, Taylor & Francis, Boca Raton
17. James, L. F., Hartley, W. J., Williams, M. C., and Van Kampen, K. R. (1980) Field and experimental studies in cattle and sheep poisoned by nitro-bearing Astragalus or their toxins. *American journal of veterinary research* **41**, 377-382
18. Francis, K., Nishino, S. F., Spain, J. C., and Gadda, G. (2012) A novel activity for fungal nitronate monooxygenase: Detoxification of the metabolic inhibitor propionate-3-nitronate. *Arch Biochem and Biophys* **521**, 84-89
19. Francis, K., Russell, B., and Gadda, G. (2005) Involvement of a flavosemiquinone in the enzymatic oxidation of nitroalkanes catalyzed by 2-nitropropane dioxygenase. *J Biol Chem* **280**, 5195-5204
20. Su, D., Kabir, M. P., Orozco-Gonzalez, Y., Gozem, S., and Gadda, G. Fluorescence Properties of Flavin Semiquinone Radicals in Nitronate Monooxygenase. *ChemBioChem* **0**
21. Inoue, H., Nojima, H., and Okayama, H. (1990) High efficiency transformation of Escherichia coli with plasmids. *Gene* **96**, 23-28
22. Bush, M. T., Touster, O., and Brockman, J. E. (1951) The production of beta-nitropropionic acid by a strain of Aspergillus flavus. *J Biol Chem* **188**, 685-693
23. Lewis, R. J. (1996) *Sax's Dangerous Properties of Industrial Materials*, 9th ed., Van Nostrand Reinhold, New York
24. Goodall, D. M., and Long, F. A. (1968) Protonation of nitroalkane anions by acetic acid in mixed water-deuterium oxide solvents. *Journal of the American Chemical Society* **90**, 238-243
25. Nielsen, A. T. (1969) *Nitronic acids and esters. In the Chemistry of the Nitro and Nitroso Groups.* , Intersciene Publishers, New York
26. Aliverti, A., Curti, B., and Vanoni, M. A. (1999) Identifying and quantitating FAD and FMN in simple and in iron-sulfur-containing flavoproteins. *Methods in molecular biology (Clifton, N.J.)* **131**, 9-23
27. Whitby, L. G. (1953) A new method for preparing flavin-adenine dinucleotide. *Biochem J* **54**, 437-442
28. Bradford, M. M. (1976) A rapid and sensitive method for the quantitation of microgram quantities of protein utilizing the principle of protein-dye binding. *Anal Biochem* **72**, 248-254
29. Orozco-Gonzalez, Y., Kabir, M. P., and Gozem, S. (2019) Electrostatic Spectral Tuning Maps for Biological Chromophores. *The Journal of Physical Chemistry B*
30. Su, D., Yuan, H., and Gadda, G. (2017) A Reversible, Charge-Induced Intramolecular C4a-S-Cysteinyl-Flavin in Choline Oxidase Variant S101C. *Biochemistry* **56**, 6677-6690
31. Macheroux, P., Massey, V., Thiele, D. J., and Volokita, M. (1991) Expression of spinach glycolate oxidase in Saccharomyces cerevisiae: purification and characterization. *Biochemistry* **30**, 4612-4619
32. Schwans, J. P., Sunden, F., Gonzalez, A., Tsai, Y., and Herschlag, D. (2013) Uncovering the determinants of a highly perturbed tyrosine pKa in the active site of ketosteroid isomerase. *Biochemistry* **52**, 7840-7855

33. Latovitzki, N., Halper, J. P., and Beychok, S. (1971) Spectrophotometric Titration of Tyrosine Residues in Human Lysozyme. *Journal of Biological Chemistry* **246**, 1457-1460
34. Cleland, W. W. (1963) The kinetics of enzyme-catalyzed reactions with two or more substrates or products: I. Nomenclature and rate equations. *Biochimica et Biophysica Acta (BBA) - Specialized Section on Enzymological Subjects* **67**, 104-137
35. Murray, M. S., Holmes, R. P., and Lowther, W. T. (2008) Active site and loop 4 movements within human glycolate oxidase: implications for substrate specificity and drug design. *Biochemistry* **47**, 2439-2449
36. Wohlfahrt, G., Witt, S., Hendle, J., Schomburg, D., Kalisz, H. M., and Hecht, H.-J. (1999) 1.8 and 1.9 A resolution structures of the Penicillium amagasakiense and Aspergillus niger glucose oxidases as a basis for modelling substrate complexes. *Acta Crystallographica Section D* **55**, 969-977
37. Xia, Z.-x., and Mathews, F. S. (1990) Molecular structure of flavocytochrome b2 at 24 Å resolution. *Journal of Molecular Biology* **212**, 837-863
38. Fu, G., Yuan, H., Li, C., Lu, C. D., Gadda, G., and Weber, I. T. (2010) Conformational changes and substrate recognition in Pseudomonas aeruginosa D-arginine dehydrogenase. *Biochemistry* **49**, 8535-8545
39. Sobrado, P., and Fitzpatrick, P. F. (2003) Identification of Tyr413 as an active site residue in the flavoprotein tryptophan 2-monooxygenase and analysis of its contribution to catalysis. *Biochemistry* **42**, 13833-13838
40. Schreuder, H. A., van der Laan, J. M., Hol, W. G. J., and Drenth, J. (1988) Crystal structure of p-hydroxybenzoate hydroxylase complexed with its reaction product 3,4-dihydroxybenzoate. *Journal of Molecular Biology* **199**, 637-648
41. Alston, T. A., Mela, L., and Bright, H. J. (1977) 3-Nitropropionate, the toxic substance of Indigofera, is a suicide inactivator of succinate dehydrogenase. *Proc Natl Acad Sci U S A* **74**, 3767-3771
42. Hamilton, B. F., Gould, D. H., and Gustine, D. L. (2000) History of 3-Nitropropionic Acid. in *Mitochondrial Inhibitors and Neurodegenerative Disorders* (Sanberg, P. R., Nishino, H., and Borlongan, C. V. eds.), Humana Press, Totowa, NJ. pp 21-33
43. Birkelund, T., Johansen, R. F., Illum, D. G., Dyrskog, S. E., Ostergaard, J. A., Falconer, T. M., Andersen, C., Fridholm, H., Overballe-Petersen, S., and Jensen, J. S. (2021) Fatal 3-Nitropropionic Acid Poisoning after Consuming Coconut Water. *Emerg Infect Dis* **27**, 278-280
44. Romero, E., and Gadda, G. (2014) Alcohol oxidation by flavoenzymes. *Biomol Concepts* **5**, 299-318
45. Ghanem, M., and Gadda, G. (2005) On the catalytic role of the conserved active site residue His466 of choline oxidase. *Biochemistry* **44**, 893-904
46. Su, D., Kabir, M. P., Orozco-Gonzalez, Y., Gozem, S., and Gadda, G. (2019) Fluorescence Properties of Flavin Semiquinone Radicals in Nitronate Monooxygenase. *Chembiochem* **20**, 1646-1652
47. Fraaije, M. W., and Mattevi, A. (2000) Flavoenzymes: diverse catalysts with recurrent features. *Trends Biochem Sci* **25**, 126-132

48. Su, D., Aguillon, C., and Gadda, G. (2019) Characterization of conserved active site residues in class I nitronate monooxygenase. *Arch Biochem Biophys* **672**, 108058
49. Gadda, G., and Sobrado, P. (2018) Kinetic Solvent Viscosity Effects as Probes for Studying the Mechanisms of Enzyme Action. *Biochemistry* **57**, 3445-3453
50. Wolfe, A. E., Thymark, M., Gattis, S. G., Fagan, R. L., Hu, Y. C., Johansson, E., Arent, S., Larsen, S., and Palfey, B. A. (2007) Interaction of benzoate pyrimidine analogues with class 1A dihydroorotate dehydrogenase from Lactococcus lactis. *Biochemistry* **46**, 5741-5753
51. Cleland, W. W. (1963) The kinetics of enzyme-catalyzed reactions with two or more substrates or products. I. Nomenclature and rate equations. *Biochim Biophys Acta* **67**, 104-137
52. Miller, M. D., and Phillips, G. N., Jr. (2021) Moving beyond static snapshots: Protein dynamics and the Protein Data Bank. *J Biol Chem* **296**, 100749
53. Battye, T. G., Kontogiannis, L., Johnson, O., Powell, H. R., and Leslie, A. G. (2011) iMOSFLM: a new graphical interface for diffraction-image processing with MOSFLM. *Acta Crystallogr D Biol Crystallogr* **67**, 271-281
54. Evans, P. R. (2011) An introduction to data reduction: space-group determination, scaling and intensity statistics. *Acta Crystallogr D Biol Crystallogr* **67**, 282-292
55. Winn, M. D., Ballard, C. C., Cowtan, K. D., Dodson, E. J., Emsley, P., Evans, P. R., Keegan, R. M., Krissinel, E. B., Leslie, A. G., McCoy, A., McNicholas, S. J., Murshudov, G. N., Pannu, N. S., Potterton, E. A., Powell, H. R., Read, R. J., Vagin, A., and Wilson, K. S. (2011) Overview of the CCP4 suite and current developments. *Acta Crystallogr D Biol Crystallogr* **67**, 235-242
56. P.V. Afonine, R. W. G.-K., N. Echols, J.J. Headd, N.W. Moriarty, M. Mustyakimov, T.C. Terwilliger, A. Urzhumtsev, P.H. Zwart, and P.D. Adams. (2012) Towards automated crystallographic structure refinement with phenix.refine. *Acta Crystallogr D Biol Crystallogr*, 381-390
57. Lide, D. R. (2000) *CRC Handbook of Chemistry and Physics*, 81st ed., CRC Press, Boca Raton, Fl

# 4 CONCLUSION

In summary, the role of Y109, Y254, Y299, Y303, and K307 residues, located in the active site of *Pa*NMO, has been elucidated. Among ~500 sequences belonging to class I NMOs, the fully conserved active site tyrosine residues in *Pa*NMO must be protonated in order to bind the negatively charged P3N substrate. Mutant enzymes containing the individual mutations Y109F, Y254F, Y299F, Y303F, and K307M were prepared to understand the effect on the single-electron transfer reaction between P3N and the flavin i.e. reductive half-reaction and the electron transfer reaction between the reduced flavin and oxygen i.e. oxidative half-reaction. There was no effect on both the reductive and oxidative half-reactions. It is currently not understood why these tyrosine and lysine residues have been conserved in the active sites of NMOs from various organisms. These residues may participate in different enzymatic reactions or simply are present to ensure P3N binding without a strict spatial arrangement.

Among ~500 sequences from various fungal, bacterial, and animal sources, H183 is a fully conserved active site residue located above the N(5) atom of the flavin cofactor. Until now, no mechanistic or structural studies have described the role of the H183 in the detoxification of P3N. H183 is essential to maintain an active enzyme-substrate complex competent for the single electron transfer reaction from P3N substrate to the flavin cofactor i.e. reductive half-reaction. Upon replacing H183 with a glutamine, an active and inactive conformation was observed kinetically and in the crystal structure of the H183Q mutant crystallized in the presence and absence of a substrate analog. The Q183 mutant sidechain blocked the N(5) atom of the flavin in the inactive conformation. In the active conformation, the substrate analog, serving as a

model for the substrate, was oriented toward the reactive center of the flavin. Using a stopped-flow spectrophotometer, an extended lag in reaction time was observed in the stopped flow traces, suggesting the presence of an isomerization between the inactive and active conformations required for the single electron transfer from the P3N substrate and the flavin cofactor.